Internally-crosslinked alginate dialdehyde/alginate/gelatin-based hydrogels as bioinks for prospective cardiac tissue engineering applications

ACCSCIENCE PUBLISHING

International Journal of Bioprinting

RESEARCH ARTICLE

Internally-crosslinked alginate dialdehyde/alginate/gelatin-based hydrogels as bioinks for prospective cardiac tissue engineering applications

Giovanni Paolo Stola[1,2], Camilla Paoletti[1,2], Letizia Nicoletti[1,2], Geo Paul[3], Claudio Cassino[3], Leonardo Marchese[3], Valeria Chiono[1,2*], and Elena Marcello[1,2*]

[1]Department of Mechanical and Aerospace Engineering, POLITO BioMedLab, Politecnico di Torino, Turin, Italy

[2]Interuniversity Center for the Promotion of the 3Rs Principles in Teaching and Research (Centro 3R), Pisa, Italy

[3]Department of Science and Technological Innovation and "Centro Interdisciplinare Nano-SiSTeMI", Università del Piemonte Orientale, Alessandria, Italy

Abstract

Cardiovascular diseases represent a global challenge due to heart-limited regenerative capabilities. 3D-bioprinted cell-laden constructs are a promising approach as cardiac patches or *in vitro* models. However, developing bioinks with optimal mechanical, rheological, and biological properties remains challenging. Although alginate (Alg)-based bioinks have been extensively explored, such hydrogels lack cell adhesion properties and degradability. Additionally, 3D Alg structures are usually obtained by microextrusion bioprinting, exploiting conventional external crosslinking methods, which introduce inhomogeneities and unpredictability in construct formation. This work exploits Alg internal ionic gelation mechanism to obtain homogeneous self-standing multilayered 3D-printed constructs without employing support baths or post-printing crosslinking treatments. Alg was blended with oxidized alginate (ADA) and gelatin (Gel) to achieve degradable and cell-adhesive hydrogels for cardiac tissue engineering. Firstly, ADA/Alg bioink composition was tailored to achieve cardiac tissue-like viscoelastic properties. Then, the amount of Gel in ADA/Alg hydrogels was optimized to support cell adhesion, producing shear thinning inks with tunable viscoelastic properties (storage modulus [G']: 650–1300 Pa) and degradation profile (40–80% weight loss after 21 days in phosphate-buffered saline [PBS]) by varying Gel concentration. ADA/Alg/Gel hydrogels displayed shear thinning behavior, suitable for 3D bioprinting depending on the ink stabilization time, due to the gradual pH-triggered release of calcium ions over time. Adult human cardiac fibroblast (AHCF) and H9C2-laden ADA/Alg/Gel bioinks were successfully printed, producing scaffolds with high shape fidelity and good cell viability post-printing. Finally, the highest Gel content (25% [w/w]) supported cell adhesion after 24 h of incubation, displaying potential for cardiac tissue modeling. This research presents a comprehensive framework for advancing the design of bioink.

Keywords: Alginate dialdehyde; Gelatin; Bioink; Internal gelation; *In vitro* cardiac models

***Corresponding authors:**
Valeria Chiono (valeria.chiono@polito.it)

Elena Marcello (elena.marcello@polito.it)

Citation: Stola GP, Paoletti C, Nicoletti L, et al. Internally-crosslinked alginate dialdehyde/alginate/gelatin-based hydrogels as bioinks for prospective cardiac tissue engineering applications. *Int J Bioprint*. 2024;10(6):4014. doi: 10.36922/ijb.4014

Received: June 21, 2024
1st revised: August 1, 2024
2nd revised: September 10, 2024
Accepted: September 18, 2024
Published Online: September 18, 2024

1. Introduction

3D bioprinting has radically transformed the manufacturing process of scaffolds for tissue engineering (TE) applications by converting computer-aided design models into layered structures, bypassing traditional molding methods.[1] Highly reproducible and customizable 3D-printed scaffolds can be employed as a potential approach to meet the increasing global demand for organ replacement and tissue regeneration.[2,3] In this scenario, the heart ranks as the third most transplanted organ worldwide, primarily because it represents the only therapeutic option in case of end-stage heart failure due to its poor intrinsic regenerative capacity. In the last three decades, cardiac TE has emerged as a potential new therapeutic and *in vitro* modeling approach, based on the use of biomaterials, eventually combined with bioactive factors, with/without cells for regeneration.[4] 3D-bioprinted constructs can be exploited as therapeutic patches[5,6] to favor heart regeneration or as *in vitro* models of human cardiac tissue for preclinical validation of drugs and therapies, in agreement with the 3Rs principles.[7]

Among 3D bioprinting techniques, microextrusion bioprinting is based on the layer-by-layer deposition of cell-laden bioinks to create intricate 3D structures. This technique has emerged as a promising tool in TE, owing to its scalability, versatility, and the capability to incorporate various cell types, growth factors, and biomolecules within the bioink matrix.[8] Microextrusion printing relies on hydrogels as ideal bioink materials for 3D printing cell-laden constructs, allowing the production of hydrated constructs mimicking the natural extracellular matrix (ECM) of tissues.[9] Despite considerable efforts, one key challenge in micro-extrusion bioprinting is the availability of suitable bioinks able to fulfill all the following requirements: (i) biocompatibility; (ii) biomimetic properties comparable to the ECM of the target tissue, in order to favor cell adhesion, spreading, and differentiation; (iii) controlled degradability, ideally matching the cell-mediated ECM deposition rate; and (iv) proper rheological characteristics for printing.[10-12]

Among the materials investigated for microextrusion bioprinting applications, alginate (Alg) has been widely employed due to its tunable properties, cost-effectiveness,[10,11] non-immunogenicity, and non-toxicity. Hence, Alg represents an excellent candidate for regenerative medicine and has been recently tested in preclinical research and clinical trials for cardiovascular diseases.[12,13] Algysil-LVR (LoneStar Heart Inc., United States of America [USA]) is an Alg-based injectable hydrogel designed for the treatment of heart failure by reshaping the left ventricle geometry, preventing or reversing ventricular enlargement.[12,14] Once injected, the biopolymer thickens and forms gel bodies that remain in the heart muscle as permanent internal support implants for the injured heart, preventing disease progression.[12,14] The device has been tested in three clinical trials: two were completed (ClinicalTrials.gov identifier: NCT00847964; NCT01311791 [AUGMENT-HF]) and one has been published but is still not recruiting (ClinicalTrials.gov identifier: NCT03082508 [AUGMENT-HF II]). However, Algysil-LVR is defined as a permanent device that only offers mechanical support to the left ventricle without providing full restoration of cardiac functionality.[12,13]

One of the most interesting properties of Alg is the ability to complex with divalent cations, particularly calcium ions, to form hydrogels through physical crosslinking under physiological conditions, forming an "egg box" model.[15] Depending on the source of calcium ions, two different modes of ionic crosslinking have been investigated: internal and external methods.[16-18] External gelation is characterized by the use of highly soluble calcium salts (i.e., $CaCl_2$) and consists of the diffusion of multivalent cations from the outside into the Alg solution phase, forming a crosslinked Alg matrix. Most studies on microextrusion bioprinting of Alg bioinks have exploited such external mechanism.[19-21] The use of external crosslinking leads to the formation of a non-homogeneous filament, characterized by a highly crosslinked surface, as the rapid gelation is confined at the interface between the calcium solution and Alg phase.[22,23] Such highly crosslinked surface might affect the behavior of embedded cells, limiting the diffusion of nutrients and oxygen.[24,25] Moreover, the application of the external crosslinking technique is usually associated with the use of coagulation baths, in which the Alg phase is extruded. Such baths (e.g., freeform reversible embedding of suspended hydrogels [FRESH] printing[19]) physically support the extruded bioink filaments and allow crosslinking of its polymeric chains to obtain constructs with high shape fidelity and resolution. However, the use of such a support bath, which involves a microparticle slurry, adds complexity to the bioprinting process, as particle size and shape can significantly affect bioprinting resolution and the morphology of the printed filaments.[26] Lastly, the use of external gelation can be a drawback for drug delivery applications, as the cargo embedded within the bioink might be partially released during the coagulation step.

Recently, internal gelation of Alg solutions has been studied to develop 3D self-standing constructs without the need for a support bath. Internal gelation involves the dispersion of water-insoluble calcium salt, such as calcium carbonate ($CaCO_3$), within the Alg solution, followed by the gradual release of calcium ions through a decrease in pH that is induced by an acidic compound, usually

D-(+)-glucono-1,5-lactone (GDL).[16,18] Internal gelation allows a more uniform distribution of multivalent cations within the Alg phase during gelation, resulting in a more homogeneous gel and allowing 3D printing of uniform self-supporting hydrogel fibers, without the need for post-crosslinking or supporting materials or baths.[27,28] However, internal crosslinking of Alg-based bioinks has been often used as a pre-crosslinking mechanism to improve the printability of the hydrogel by increasing its viscosity.[22,29] Hence, in such studies, an external gelation mechanism has been added to fully crosslink the construct and improve hydrogel stability. The application of the secondary external crosslinking mechanism can lead to the release of water-soluble components present in the bioink, such as proteins (e.g., gelatin or collagen) or small hydrophilic molecules (added for drug release applications).[27,30] Limited research has been conducted on solely utilizing internal crosslinking to print self-standing uniform Alg-based 3D constructs.[27,28] Remaggi et al. investigated the printability of Alg bioinks with $CaCO_3$ and GDL to be used as a platform for the delivery of Epirubicin, a water-soluble drug for the treatment of breast cancer.[27] However, in that study, selected printing conditions comprised a curing time of three days at 2°C, which is not suitable for *in vitro* cell cultures. Sardelli et al. performed an extensive investigation on the printability of Alg inks by internal gelation, exploring the rheological properties of the material and fiber printability.[28] Guagliano et al. recently developed a bioink composed of internally crosslinked Alg and ECM for bioprinting volumetric hepatic tissue models. The scaffold design was optimized to achieve 14-layered printed constructs using internal gelation alone, demonstrating the bioink capability to support mid/long-term cultures of human liver cancer cells (HepG2) in static conditions for up to 12 days.[31-33]

Although Alg has been extensively used for biomedical applications, it is limited by two main drawbacks: (i) poor *in vivo* degradability due to the lack of enzymes in mammals that can induce the degradation of Alg, and (ii) lack of adhesive moieties for cells.[10,11] To overcome the first drawback, Alg dialdehyde (ADA), an oxidized form of Alg, has been obtained by partial oxidation with sodium metaperiodate.[34,35] Literature studies suggested that ADA has a lower molecular weight (MW) compared to Alg, and its degradation occurs by alkaline β-elimination.[34,35] To improve cell adhesion and proliferation, Alg hydrogels have been previously blended with gelatin (Gel)[36,37] and stabilized by an external physical gelation or a double crosslinking mechanism via chemical reactions (i.e., Schiff base formation between the aldehyde groups of ADA and the amino groups of Gel) and external ionic gelation.[36,38,39] Recently, Heid et al. evaluated the possibility of printing ADA/Gel hydrogels via an internal crosslinking mechanism through the incorporation of bioactive inorganic fillers that can slowly release bivalent calcium ions.[40] Nevertheless, the addition of external gelation was necessary to achieve well-defined 3D-printed ADA/Gel constructs, and internal gelation only improved ADA/Gel *in vitro* stability for long periods (i.e., up to 21 days).

The novelty of this work lies in the combination of ADA, Alg, and Gel hydrogels with an internal crosslinking mechanism to develop bioinks for prospective applications in *in vitro* cardiac TE. Although studies have already investigated the use of internal gelation for Alg bioprinting,[28,32,33] we reported the possibility of exploiting such crosslinking for ADA-based hydrogels, in combination with Alg and Gel, with ADA as the main component. Moreover, we investigated the possibility of applying these materials for the development of self-standing homogeneous structures for future applications in cardiac TE. Firstly, ADA/Alg hydrogel composition was optimized by varying the content of calcium ions ($CaCO_3$) and GDL to achieve cardiac tissue-like viscoelastic properties. Then, the amount of Gel in ADA/Alg hydrogels was optimized to achieve tunable viscoelastic and degradation properties, cytocompatibility, and cell-adhesive properties. All hydrogel formulations were characterized through rheological and *in vitro* degradation studies. Three gelatin concentrations were then selected for 3D microextrusion printing, and material printability was investigated over time to evaluate the effect of time-dependent pH-triggered release of calcium ions. Specifically, the composition and crosslinking kinetics were fine-tuned to achieve an optimal printability window suitable for application in 3D bioprinting (i.e., 15–90 min) without using curing or post-processing strategies. *In vitro* biocompatibility of the three hydrogel systems was investigated using adult human cardiac fibroblasts (AHCFs). Finally, as a proof of concept for cardiac TE applications, bioprinting of AHCF-laden and H9C2-laden hydrogels was investigated, and cell viability after printing was studied.

2. Materials and methods

2.1. Materials

Sodium Alg (alginic acid sodium salt, medium viscosity) was purchased from MP Biomedicals (USA). Calcium carbonate ($CaCO_3$), GDL (C6H1006), potassium iodide (KI), and soluble starch solution were obtained from Alfa Aesar (USA). Sodium metaperiodate ($NaIO_4$; MW: 213.98), sodium chloride (NaCl), Gel (Bloom 300, Type A, porcine skin, suitable for cell culture), 2,4,6-trinitrobenzene sulfonate (TNBS), tert-butyl carbazate (t-BC), phosphate-buffered saline (PBS) tablets, and Trypsin/EDTA solution were supplied from Sigma-Aldrich (USA). Dialysis

membrane tubings were acquired from Spectrum Lab (Spectrum™ Spectra/Por™, New Zealand), based on regenerated cellulose with MW cut-off (MWCO) of 6–8 kDa. Ethanol absolute, anhydrous ethylene glycol and hydrochloric acid (37% [w/v]) were obtained from Carlo Erba (Italy). Dulbecco's modified Eagle medium (DMEM), fetal bovine serum (FBS), sodium pyruvate, and L-glutamine solution were acquired from GIBCO (USA). CellTiter Blue and CytoTOX-ONE™ assay were acquired from Promega (USA). Live/Dead™ Viability/Cytotoxicity Kit was obtained from Invitrogen (USA).

2.2. Production and characterization of alginate dialdehyde

2.2.1. Production of alginate dialdehyde

Alginate dialdehyde (ADA) was prepared by controlled oxidation of sodium Alg via sodium metaperiodate according to the protocol by Sarker et al.[41] Briefly, a 20% (w/v) sodium Alg dispersion in ethanol was prepared and stirred for 1 h at room temperature. A 0.3 M solution of sodium metaperiodate in deionized water was then added dropwise to the sodium Alg dispersion under magnetic stirring in the dark at room temperature. After 6 h, the reaction was quenched by adding 0.2% (v/v) ethylene glycol solution under continuous stirring for 30 min. The resulting solution was dialyzed (Spectrum™ Spectra/Por™ membrane; MWCO: 6–8 kDa) in deionized water for seven days to remove all traces of unreacted sodium metaperiodate and then lyophilized.

Two methods were used to determine ADA degree of oxidation: an indirect and a direct method. For the indirect method, the degree of oxidation was determined by measuring the unreacted sodium metaperiodate before quenching the reaction with ethylene glycol. A soluble starch indicator solution was prepared by mixing equal volumes of KI (20% [w/v]) and soluble starch (1% [w/v]) solutions using PBS as the solvent. Reaction mixture (1 mL) was added to 250 mL of deionized water. Then, 3 mL of the diluted solution was mixed with 1.5 mL of indicator solution and 0.5 mL of distilled water. The absorbance of the tri-iodine-starch complex was measured using a UV-Vis spectrophotometer (Varioskan LUX multimode microplate, Thermofisher, Italy) at 486 nm. The concentration of periodate in the sample was obtained using a calibration curve previously obtained with different concentrations of sodium metaperiodate (0.0016–0.02 mg/mL). The difference between the initial and final amount of sodium metaperiodate corresponds to the hydroxyl groups converted into aldehyde groups.

For the direct method, the quantification of aldehyde groups was performed using the TNBS assay, following a protocol described by Wang et al.[42] Briefly, 25 µL of ADA solution (1% [w/v]) was mixed with 25 µL t-BC (30 mM in acetic acid) and allowed to react overnight. Subsequently, 0.5 mL of TNBS solution (6 mM in 0.1 M sodium bicarbonate) was added and allowed to react for 1 h. The reaction was quenched by adding 0.55 mL of HCl (0.5 N), and the absorbance was measured at 340 nm using the UV-Vis spectrophotometer (Varioskan LUX multimode microplate, Thermofisher, Italy). The concentration of unreacted t-BC was calculated using a calibration curve obtained using t-BC standards and aldehyde groups determined by calculating the reacted t-BC.

2.2.2. Determination of viscosity average molecular weight

The viscosity average molecular weight (Mv) of Alg and ADA was determined by viscometric analysis using an Ubbelohde viscometer (Poulten Selfe & Lee Limited, England).[43] Briefly, Alg and ADA solutions were prepared at different concentrations (0.025–0.2 and 0.2–0.6% [w/v], respectively). Inherent and reduced viscosity were calculated and plotted against concentration. Finally, after checking the linearity, the intrinsic viscosity (η) was derived, and Mv was calculated according to the Mark-Houwink-Sakurada equation (Equation I).[44]

$$[\eta] = K\,\mathrm{Mv}^{\alpha} \quad \text{(I)}$$

where $K = 0.0073 cm^3/g$ and $\alpha = 0.92$ are the Mark-Houwink-Sakurada parameters considered for Alg and ADA.[44]

2.2.3. Attenuated total reflectance Fourier transform infrared spectroscopy

Attenuated total reflectance Fourier transform infrared (ATR-FTIR) was carried out to investigate the formation of aldehyde groups in the Alg chains. The analyses were performed in a spectral range of 4000–600 cm^{-1} with a resolution of 4 cm^{-1} using ATR-FTIR Frontier FT-IR Perkin Elmer instrument (PerkinElmer Inc., USA).

2.2.4. Nuclear magnetic resonance spectroscopy analysis

^{13}C cross polarization under magic angle spinning (CP-MAS) nuclear magnetic resonance spectroscopy (NMR) of Alg powder and ADA lyophilized samples was performed using a Bruker AVANCE III HD NMR spectrometer (Bruker, Germany) equipped with an 11.74 T superconducting magnet (500 MHz ^{1}H Larmor frequency; Bruker, Germany) to investigate the presence of aldehyde groups. Moreover, Alg and ADA block composition (M/G ratios) was calculated from ^{13}C CP-MAS NMR spectra deconvoluted using Gaussian and/or Lorentzian line

shapes.[45] Thus, the M/G ratio was estimated according to **Equation II**:

$$\frac{M}{G}ratio = \frac{E+F}{D+G+H} \quad \text{(II)}$$

where E and F are the integrated intensities of signals at 76.4 and 71.6 ppm, respectively, to estimate the mannuronate content; and D, G, and H are the integrated intensities of signals at 82.8, 68.4, and 65.5 ppm, respectively, to estimate the guluronate content.

2.3. Hydrogel composition and preparation

All the hydrogels were obtained using a dual-syringe mixing method starting from 8% (w/v) Alg, ADA, and Gel stock solutions in PBS.

2.3.1. ADA/Alg hydrogels

The ADA/Alg hydrogels were optimized by varying the ADA:Alg polymer ratio (2:1 and 1:1) and the final $CaCO_3$ concentration (1.5, 3, and 6%), while keeping the GDL content (5% [w/v]) and the final polymer concentration (6% [w/v]) constant, as described in **Table 1**. Hydrogels were prepared in subsequential steps using the dual-syringe luer-lock mixing method. Firstly, ADA and Alg solutions were mixed according to the specific ratio; $CaCO_3$ in powder form was then added and mixed thoroughly. Finally, an aqueous GDL solution was added to the ADA/Alg/$CaCO_3$ systems at a fixed proportion of 1:4 (GDL volume: total volume).

The GDL content was then optimized on ADA/Alg_50/50_C6 hydrogels by varying the final GDL concentration (1, 1.5, 2, 2.5, and 5% [w/v]), keeping the total polymer (6% [w/v]) and $CaCO_3$ concentrations (6% [w/v]) constant.

2.3.2. ADA/Alg/Gel hydrogels

Gelatin (Bloom 300, Type A, porcine skin; Merck, USA) was added to selected ADA/Alg_50/50 samples with 6% (w/v) $CaCO_3$ and 1.5% (w/v) GDL final concentration. The Gel content of ADA/Alg/Gel samples was optimized, keeping the final ADA concentration at 3% (w/v) and varying Alg:Gel polymer weight ratios from 100:0 to 50:50 (w/w), while maintaining the final concentration of Alg/Gel at 3% (w/v), as described in **Table 2**. ADA/Alg/Gel hydrogels were produced as described in **Section 2.3.1** using the dual-syringe luer-lock mixing method. Specifically, Gel solution was mixed with ADA/Alg blend solution before the addition of $CaCO_3$.

2.4. Rheological characterization

The rheological characterization of hydrogels (2 mm height) was performed at 37°C using an MCR 302 rheometer (Anton Paar, Austria) equipped with a parallel plate geometry (25 mm diameter). Oscillatory time sweep analyses were performed immediately after component mixing at a frequency of 5 Hz and a strain of 1% to evaluate the gel point of the hydrogels. The gel point was calculated as the time in which storage modulus (G′) is equal to loss modulus (G″). Strain sweep analyses of hydrogels (2 mm height) were performed 2 h after hydrogel formation to ensure the complete crosslinking at a frequency of 5 Hz, varying the strain from 0.1 to 100% to determine the linear viscoelastic (LVE) region. Frequency sweep analyses of hydrogels (2 mm height) were performed 2 h after hydrogel formation to ensure the complete crosslinking at a constant strain of 1%, varying the frequency from 0.1 to 100 rad/s, and were used to determine G′ and G″. The tests were performed in triplicate. Frequency analyses were used to estimate the elastic modulus (E), according to **Equation III**[46]:

$$E = 2G \cdot (1 + \nu) \quad \text{(III)}$$

where ν is the Poisson's ratio (i.e., 0.5 for alginate) and G is the storage modulus at 1 rad/s. Shear rate sweep tests were performed immediately after component mixing to investigate the non-Newtonian behavior of bioinks. Apparent viscosity (η) was recorded at selected time points

Table 1. Composition of tested ADA/Alg hydrogels with varying ADA:Alg polymer ratio and $CaCO_3$ (%w/v) concentration.

Code	Composition (wt%)		Final concentration (% [w/v])			
	ADA	Alg	ADA	Alg	$CaCO_3$	GDL
ADA/Alg_66/33_C1.5	66.6	33.3	4	2	1.5	5
ADA/Alg_66/33_C3	66.6	33.3	4	2	3	5
ADA/Alg_66/33_C6	66.6	33.3	4	2	6	5
ADA/Alg_50/50_C3	50	50	3	3	3	5
ADA/Alg_50/50_C6	50	50	3	3	6	5

Note: GDL (5% [w/v]) and total polymer (6% [w/v]) concentrations were kept constant. Abbreviations: ADA: Alginate dialdehyde; Alg: Alginate; GDL: D-(+)-glucono-1,5-lactone.

Table 2. ADA/Alg/Gel hydrogel compositions investigated.

Code	Composition (wt.%)			Final concentrations (% [w/v])				
	ADA	Alg	Gel	ADA	Alg	Gel	$CaCO_3$	GDL
ADA/Alg/Gel_50/50/0	50	50	0	3	3	0	6	1.5
ADA/Alg/Gel_50/47.5/2.5	50	47.5	2.5	3	2.85	0.15	6	1.5
ADA/Alg/Gel_50/45/5	50	45	5	3	2.7	0.3	6	1.5
ADA/Alg/Gel_50/40/10	50	40	10	3	2.4	0.6	6	1.5
ADA/Alg/Gel_50/35/15	50	35	15	3	2.1	0.9	6	1.5
ADA/Alg/Gel_50/30/20	50	30	20	3	1.8	1.2	6	1.5
ADA/Alg/Gel_50/25/25	50	25	25	3	1.5	1.5	6	1.5

Note: The final content of ADA was kept constant at 3% (w/v); Alg:Gel polymer weight ratios varied from 100:0 to 50:50; the final content of Alg+Gel was equivalent to 3% (w/v); the final concentrations of $CaCO_3$ and GDL were 6 and 1.5% (w/v), respectively. Abbreviations: Gel: Gelatin; ADA: Alginate dialdehyde; Alg: Alginate; GDL: D-(+)-glucono-1,5-lactone.

(2, 10, 20, 30, 45, 60, and 90 min) by varying the shear rate from 0.1 to 500 1/s to investigate the flow properties of the ink during extrusion.

2.5. *In vitro* stability studies

In vitro stability analysis of ADA/Alg/Gel hydrogels was performed upon incubation in PBS at 37°C. Samples (0.5 mL) were incubated in 500 µL PBS for 1, 5, 7, 14, and 21 days. At each time point, the weight of the wet hydrogel ($w_{s,t}$) was measured; the samples were then frozen at −20°C, lyophilized, and weighed again ($w_{d,t}$). The wet weight variation percentage is defined in **Equation IV**:

$$Wet\ weight\ variation(\%) = \frac{w_{s,t} - w_{s,0}}{w_{s,0}} \times 100 \quad \text{(IV)}$$

where $w_{s,t}$ is the weight of the swollen hydrogel and $w_{s,0}$ the initial wet weight of the hydrogel. The dry weight loss percentage at the time *i* was calculated using **Equation V**:

$$Dry\ weight\ loss(\%) = \frac{w_{d,0} - w_{d,t}}{w_{d,0}} \times 100 \quad \text{(V)}$$

where $w_{d,t}$ and $w_{d,0}$ are the weight of the dried hydrogel at time *t* and 0, respectively.

2.6. Printing process and printability evaluation

The printability of hydrogels was evaluated using the RegenHU – 3DDiscovery™ bioprinter (RegenHU, Switzerland) upon optimizing printing parameters. All printability tests were performed using cylindrical nozzles (250 µm inner diameter), at 37°C, a printing speed of 15 mm/s, and minimal pressure (30–70 kPa) for continuous filament deposition.

To investigate hydrogel printability as a function of time, ADA/Alg/Gel_50/50/0, ADA/Alg/Gel_50/40/10, and ADA/Alg/Gel_50/25/25 were printed at selected time points (10, 20, 30, 45, 60, and 90 min) into square grid structures (15 × 15 mm^2), with strand spacing of 2.5 mm. Brightfield images (4× magnification) were taken using a Nikon Eclipse Ti2 spinning disk confocal microscope equipped with NIS-Elements software (Nikon, Japan), and data were analyzed by ImageJ software. At the selected time points, two grids for each composition were printed; for each grid, five images were taken. The filament width of the printed structures was measured in five different locations for each collected image. Moreover, the filament spreading ratio (S),[47] defined as the width of the printed filament divided by the needle diameter, and the printability index (Pr),[48] defined by comparing the circularity of a square ($\pi/4$) with the outcome pores, were measured for each bioink at each time point using **Equations VI** and **VII**:

$$Spreading\ ratio(S) = \frac{width\ of\ the\ printed\ filament}{nozzle\ diameter} \quad \text{(VI)}$$

$$Printability\ index(Pr) = \frac{Pore\ perimeter^2}{16\ Pore\ Area} \quad \text{(VII)}$$

Finally, to assess the possibility of developing self-standing internally crosslinked structures using the optimized bioink, ADA/Alg/Gel_50/25/25 formulation was printed into 3D grid structures with square mesh geometry (strand distance: 5 mm), obtaining 3D square samples (10 × 10 mm^2; five layers), and into hollow 3D cylindrical structures (diameter ∅: 3 mm; 10 layers).

2.7. *In vitro* biological characterization

2.7.1. Cell culture

AHCFs were purchased from Lonza (CC-2903; Lonza, Switzerland) and maintained in culture using Fibroblasts Growth Medium-3 (PromoCell, Germany) containing 10% FBS, 1% (v/v) insulin, 1% (v/v) human basal fibroblast growth factor (hFGF-B), and 1% (v/v) gentamicin. Cells were expanded until the fourth passage and then used for experiments. H9C2 heart myoblasts were purchased from the American Type Culture Collection (ATCC, USA) and maintained in culture using DMEM, supplemented with 10% FBS, 2% L-glutamine, 1% sodium pyruvate, and 1% penicillin/streptomycin.

In vitro experiments with AHCFs were conducted in complete medium composed of DMEM, supplemented with 10% FBS, 1% L-glutamine, and 1% penicillin/streptomycin, at 37°C in 5% CO_2 atmosphere. *In vitro* experiments with H9C2 were conducted in a complete medium composed of DMEM, supplemented with 10% FBS, 2% L-glutamine, 1% sodium pyruvate, and 1% penicillin/streptomycin.

2.7.2. Indirect cell viability and cytotoxicity assays

In vitro cell viability by indirect contact with ADA/Alg/Gel_50/50/0, ADA/Alg/Gel_50/40/10, and ADA/Alg/Gel_50/25/25 hydrogels was studied using AHCFs following ISO 10993. AHCFs were seeded in a tissue culture 96-well at a cell density of 6×10^3 cells/well in a complete medium and maintained in a humified incubator at 37°C and 5% CO_2. For each sample, hydrogels with 6.4 mm diameter and 2 mm thickness were prepared and incubated (37°C and 5% CO_2) with 500 µL medium per 100 mg hydrogel for 24 h. Eluates were then collected and added to the AHCF cultures. Then, AHCFs were cultured for 24 h at 37°C with 5% CO_2. After 24 h, cell viability and cytotoxicity were measured using Cell TiterBlue and CytoTox-ONE™ assay, respectively. For cell viability, the control group consists of cells cultured in fresh complete medium. For cytotoxicity, the control group consists of cells cultured in fresh complete medium and treated with CytoTox-ONE™ lysis solution (to achieve 100% cell death) according to manufacturer instructions. Samples were analyzed using a Varioskan spectrophotometer (Thermofisher, Italy) at excitation and emission wavelengths of 560 and 590 nm, respectively.

2.7.3. Cell printing

Bioprinting of ADA/Alg/Gel_50/50/0, ADA/Alg/Gel_50/40/10, and ADA/Alg/Gel_50/25/25 hydrogels embedding AHCFs was investigated. Briefly, cultured AHCFs were detached using 0.05% Trypsin/EDTA and centrifuged. The cell pellet was resuspended in PBS and incorporated into bioinks at a concentration of 5×10^5 cells/mL. Subsequently, for each bioink composition, two-layered grid structures (10×10 mm^2) with 2 mm strand spacing were printed using a RegenHU-3DDiscovery™ bioprinter (RegenHU, Switzerland) with optimized parameters, including the printability window. Cell viability was investigated using the live/dead assay at 1 and 24 h post-printing by culturing constructs in complete media at 37°C with 5% CO_2.

As a proof-of-concept for cardiac TE, bioprinting of ADA/Alg/Gel_50/25/25 embedding H9C2 was investigated. Cultured H9C2 were detached using 0.05% Trypsin/EDTA and centrifuged. The cell pellet was resuspended in PBS and incorporated into bioinks at a concentration of 5×10^5 cells/mL. Subsequently, two-layered grid structures (10×10 mm^2) with 5 mm strand spacing were printed using the RegenHU-3DDiscovery™ bioprinter (RegenHU, Switzerland) with optimized parameters, including the printability window. Cell viability was investigated using the live/dead assay at 1 and 24 h post-printing by culturing constructs in complete media at 37°C with 5% CO_2.

2.8. Statistical analysis

All measurements were made in triplicate, and data are presented as the mean ± standard deviation. One-way analysis of variance (ANOVA) was performed with GraphPad Prism 6 software; differences were considered statistically significant at $p < 0.05$. Tukey post-hoc test was conducted between two or more groups to determine if there were statistically significant differences between populations. In particular, $^*p < 0.05$, $^{**}p < 0.01$, $^{***}p < 0.001$, and $^{****}p < 0.0001$.

3. Results and discussion

This work aimed to develop novel bioinks based on a combination of ADA with Alg and Gel, exploiting an internal crosslinking mechanism to achieve 3D-printed cell-supporting and self-standing constructs without the need for a support bath or external crosslinking. Alg-based hydrogels were selected, as Alg has already been widely investigated for biomedical applications, specifically in cardiac regeneration.[12,20] In this work, ADA was employed to improve the degradability of Alg. Firstly, ADA was combined with Alg, and internal crosslinking was exploited to achieve cardiac tissue-like viscoelastic properties, tailoring both the ADA/Alg ratio and calcium ion ($CaCO_3$) content. GDL content was then optimized to reduce potential detrimental effects on cell viability caused by environmental acidification. Then, the incorporation of Gel within the ADA/Alg hydrogels was optimized to improve cytocompatibility and impart cell adhesive properties. Printability of ADA/Alg/Gel bioinks was investigated over time to evaluate the effect of time-dependent pH-triggered release of calcium ions. Finally,

bioprinting of AHCFs-and H9C2/laden hydrogels was investigated, and cell viability after printing was studied.

3.1. ADA production and characterization

Alginate dialdehyde (ADA) was prepared via oxidation of Alg using sodium metaperiodate, achieving a production yield of 70 ± 5%. Oxidation reaction causes the cleavage of a carbon–carbon bond and the formation of two aldehyde groups.[49,50] Following previous literature reports,[41,50] a theoretical oxidation degree of 25% was targeted by controlling the stoichiometric addition of $NaIO_4$. ADA oxidation degree was measured by both indirect and direct methods. The indirect method was used as a preliminary assessment of the oxidation degree by measuring the amount of unreacted sodium metaperiodate.[41,51] As 99% sodium metaperiodate was consumed in the reaction, the theoretical oxidation degree was calculated to be 23 ± 1%. Conversely, the direct method is based on the direct quantification of aldehyde groups in ADA using the TNBS assay. This method yielded an oxidation degree of 25 ± 4% (mol aldehyde group/mol polymer).

The initial chemical characterization of ADA and Alg was analyzed using ATR-FTIR (Figure 1A). ATR-FITR spectra of Alg and ADA displayed the typical absorption bands of the Alg structure: 1318 cm^{-1} due to C-O stretching; 1126 cm^{-1} indicating C-C stretching; 1021 cm^{-1} attributed to C-O-C stretching; 1590 and 1414 cm^{-1} due to the asymmetric and symmetric stretching vibrations of carboxylate salt groups (-C=(O)O-) of Alg.[41] In the ADA ATR-FTIR spectrum, additional bands with very low intensity were detected at 2850 and 1740 cm^{-1} associated respectively with the C-H and C=O vibrations in aldehyde groups suggesting successful ADA production.[41]

To further assess aldehyde group formation, ^{13}C CP-MAS NMR spectroscopy was performed on Alg and ADA lyophilized samples (Figure 1B). Both Alg and ADA spectra displayed peaks associated with the carbon atoms present in mannuronate (M1: 99.5 ppm; M2, M3: 71.6 ppm; M4, M5: 76.4 ppm; M6: 172.6 ppm) and guluronate (G1: 102.2 ppm; G2: 65.5; G3, G5: 68.4 ppm; G4: 82.8 ppm; G6: 172.6 ppm).[52] The spectra of ADA exhibited an additional peak at 92.2 ppm, attributed to hemiacetalic groups originating from aldehydic groups.[53] Moreover, the resonance of both M-6 and G-6 at 176.2 ppm, attributed to carboxylate groups, were not altered, proving that sodium metaperiodate can convert diols to aldehydes without affecting the carboxylate groups.[53] Deconvolution of the ^{13}C CP-MAS-NMR (Figure S1A and B, Supporting Information) spectra of Alg and ADA allow to determine the M/G ratio in both polymers; 1.2 ± 0.3 for Alg and 1.5 ± 0.5 for ADA. ADA displayed a slight reduction of G groups compared to Alg, though no significant differences were detected in the M/G ratio between the two materials. Literature studies have

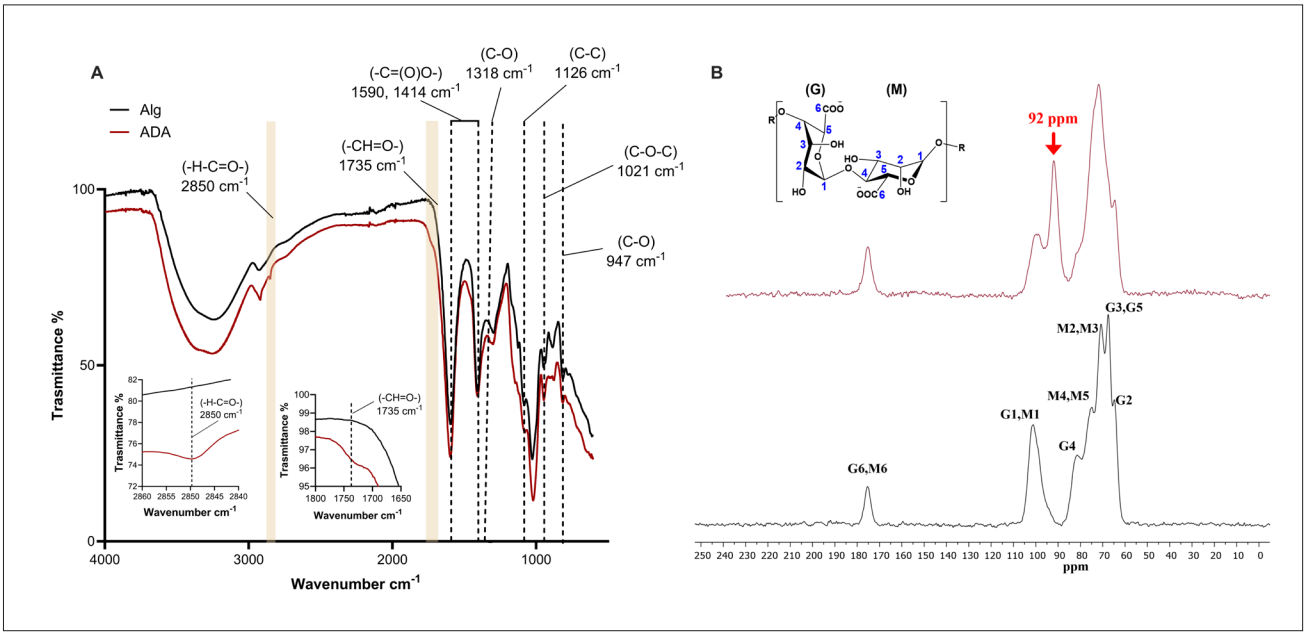

Figure 1. Characterization of ADA and Alg (A) Attenuated total reflectance Fourier transform infrared (ATR-FTIR) spectra of alginate (Alg; black) and lyophilized Alg dialdehyde (ADA; red). The inset figures represent magnifications of the spectra areas at 2840–2860 cm^{-1} (left) and 1650–1800 cm^{-1} (right). (B) ^{13}C cross polarization under magic angle spinning nuclear magnetic resonance (CP-MAS NMR) spectra of Alg (black) and lyophilized ADA (red). G and M represents guluronate and mannuronate groups, respectively.

reported contradictory results on the effect of oxidation on G and M groups, suggesting either a preferential reaction of G groups to oxidation[52,53] or no difference between the two groups.[54] Differences in the results might be associated with the different M/G ratios of the starting Alg being oxidized and other factors, such as M and G block distribution.

Finally, ADA Mv was calculated to be 22 ± 1 kDa based on the Mark-Houwink-Sakurada equation, corresponding to a 93.5% reduction relative to Alg Mv (340 ± 5 kDa). Oxidation by sodium periodate triggers the scission of polysaccharide chains, causing a decrease in ADA MW and intermolecular interactions.[55] Coherently to the literature, MW reduction between 80 and 90% was thus expected with an oxidation degree of 25–30%.[51,56]

3.2. ADA/Alg-based hydrogels

The ADA/Alg samples were first optimized by varying the Alg:ADA ratio, as well as $CaCO_3$ and GDL concentrations, to obtain suitable stiffness for potential cardiac TE applications. Hydrogels with the compositions reported in Table 1 were characterized through frequency sweep tests. Initially, the influence of the Alg:ADA ratio and calcium concentration was studied at fixed GDL content (Figure 2A and B). As displayed in Figure 2A, all compositions exhibited higher G′ than G″, demonstrating their hydrogel state. G′ increased as a function of both Alg content and $CaCO_3$ concentration (Table S2, Supporting Information). At 3% (w/v) $CaCO_3$, samples with the highest Alg content (ADA/Alg_50/50_C3) exhibited higher G′ compared to ADA/Alg_66/33_C3 ($p < 0.0002$). Indeed, Alg is primarily responsible for the internal crosslinking mechanism of ADA/Alg hydrogels. ADA has a reduced ability to undergo crosslinking with calcium ions due to the chemical modification of its chains and reduced MW.[50,51,57] Ring-opening of ADA chains upon oxidation weakens or even hinders ionic crosslinking, which requires the presence of approximately 20 consecutive guluronate groups for forming egg-box ionic junctions with calcium ions.[34,58] In this work, an initial characterization of ADA (data not shown) confirmed its low ionic crosslinking ability in the presence of $CaCO_3$ and GDL, as suggested by the formation of soft hydrogels with low G′ (< 100 Pa) even at high polymer concentrations (i.e., 10% [w/v]).

At the same Alg:ADA ratio, hydrogels with higher calcium content (i.e., ADA/Alg_50/50_C6) exhibited higher G′ compared to those with lower $CaCO_3$ content (i.e., ADA/Alg_50/50_C3) ($p < 0.0001$). Overall, the ADA/Alg_50/50_C6 composition was selected as it displayed the

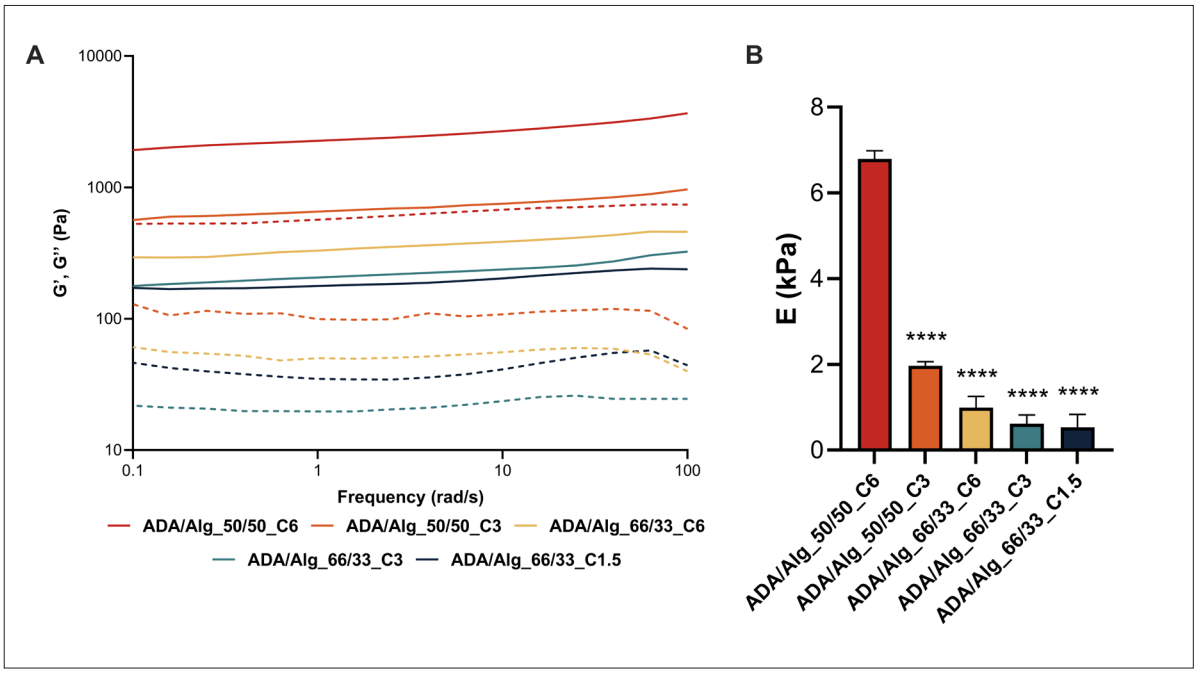

Figure 2. Rheological analysis of Alg/ADA hydrogels. (A) Storage modulus (G′; continuous line) and loss modulus (G″; dotted line) of ADA/Alg_50/50_C6 (red), ADA/Alg_50/50_C3 (orange), ADA/Alg_66/33_C6 (yellow), ADA/Alg_66/33_C3 (light blue), and ADA/Alg_66/33_C1.5 (blue) as a function of angular frequency (0.1 and 100 rad/s) at 37°C ($n = 3$). (B) Elastic modulus (E) of ADA/Alg_50/50_C6 (red), ADA/Alg_50/50_C3 (orange), ADA/Alg_66/33_C6 (yellow), ADA/Alg_66/33_C3 (light blue), and ADA/Alg_66/33_C1.5 (blue), derived from frequency sweep tests ($n = 3$). **** $p < 0.0001$ indicates a statistically significant difference with ADA/Alg_50/50_C6. Abbreviations: Alg: Alginate; ADA: Alginate dialdehyde.

closest G′ (2300 ± 65 Pa) to that of Algysil-LVR,[59] the Alg-based hydrogel currently investigated in cardiac clinical trials. Moreover, ADA/Alg_50/50_C6 exhibited an average E (derived from **Equation III**) of 6.8 ± 0.2 kPa (Figure 2B**;** Table S2, Supporting Information), which is within the range of embryonic cardiac tissue stiffness (≈1–6 kPa)[60] and close to that of adult tissue (≈10–30 kPa).[61]

The influence of GDL on ADA/Alg_50/50_C6 composition was then investigated. GDL hydrolysis into gluconic acid leads to the release of protons, which in turn induces the gradual release of calcium ions from $CaCO_3$ particles.[62] Therefore, GDL content in the matrix needs to be tailored to trigger the release of calcium ions from $CaCO_3$. However, the decrease in pH should not have a detrimental effect on cell viability[63] and should be maintained within physiological values. Hydrogels with five different concentrations of GDL (1, 1.5, 2, 2.5, and 5% [w/v])) were characterized for their rheological properties. Time sweep analysis was performed to evaluate the influence of GDL on crosslinking kinetics. As presented in Figure 3E and Table S1, Supporting Information, an increase in GDL content caused a reduction in crosslinking time (defined as the time in which G′ = G″).[18,27,62] Frequency sweep tests were performed in the LVE region, and the results are reported in Figure 3A and Table S3, Supporting Information. Elastic modulus values for all the samples were derived from the rheological data and reported in Figure 3B and Table S3, Supporting Information. Samples with reduced GDL concentration (1 and 1.5% [w/v]) expressed a significant G′ (and consequently E) decrease compared to the sample with the highest GDL amount (5% [w/v]) ($p < 0.0021$ and $p < 0.0001$ for *GDL1* and *GDL1.5*, respectively).

The pH of eluates from hydrogels with increasing GDL content was measured over time (i.e., after 1, 5, 7, 14, and 21 days). The pH variation is reported in Figure 3C and D. The composition with the highest GDL concentrations (i.e., 5, 2.5, and 2% [w/v]) exhibited a rapid pH decrease after one day of incubation (6.1 ± 0.2, 6.2 ± 0.1, and 6.56 ± 0.03, respectively), and physiological values of pH (i.e., 7.4) were achieved only after seven days. In contrast, compositions with a lower content of GDL (1.5 and 1% [w/v]) displayed a smaller decrease in pH after one day (6.78 ± 0.04 and 6.8 ± 0.02, respectively; $p < 0.0001$). Additionally, the pH of the supernatant for these compositions returned to physiological levels within five days of incubation.

Based on the rheological properties and pH variation study, hydrogel composition with 3% (w/v) Alg, 3% (w/v) ADA, 6% (w/v) $CaCO_3$, and 1.5% (w/v) GDL was selected as optimal. This formulation displayed an average G′ of 1.5 kPa (corresponding to an E of 4.5 kPa), suitable for cardiac TE applications while maintaining the pH close to *in vitro* physiological values.

3.3. ADA/Alg/Gel hydrogels

We then investigated the possibility of introducing Gel into the optimized ADA/Alg composition to improve cell adhesion. ADA/Alg/Gel hydrogels with constant 50% ADA composition were optimized by varying the Alg:Gel relative weight ratios from 50:0 to 25:25, while maintaining their overall amount at 50% (Table 2).

3.3.1. Rheological characterization

The ADA/Alg/Gel hydrogels were characterized for their rheological properties by evaluating the G′ and G″ values as a function of time (time sweep), strain (strain sweep), and frequency (frequency sweep) at 37°C.

Time sweep analysis showed that the introduction of Gel caused a faster gelation: the gel point, evaluated as the crossover of G′ and G″ curves versus time, could not be detected (data not shown) as the materials were already in a gel state (G′ higher than G″).

Frequency sweep tests were performed within the LVE range of each hydrogel to evaluate the influence of Gel on the viscoelastic behavior of the hydrogels. As displayed in Figure 4A, all hydrogels expressed a G′ higher than G″, demonstrating viscoelastic solid-like properties. Samples with the lowest Gel contents (ADA/Alg/Gel_50/47.5/2.5 and ADA/Alg/Gel_50/45/5) exhibited an average G′ (1300 ± 190 Pa and 1170 ± 115 Pa at 1 rad/s, respectively) similar to that of ADA/Alg/Gel_50/50/0, with no statistically significant differences. In contrast, hydrogel samples with a Gel content higher than 10% (ADA/Alg/Gel_50/40/10, ADA/Alg/Gel_50/35/15, ADA/Alg/Gel_50/30/20, and ADA/Alg/Gel_50/25/25) expressed a G′ significantly lower than ADA/Alg/Gel_50/50/, with ADA/Alg/Gel_50/25/25 reaching the lowest G′ value of 650 ± 55 Pa ($p < 0.0001$, when compared to ADA/Alg/Gel_50/50/0). Based on G′ from the frequency sweep analysis, the E of ADA/Alg/Gel samples was calculated to range between 2.0 ± 0.2 and 3.9 ± 0.6 kPa (Figure 4B**;** Table S4, Supporting Information). Such values are still within the range of embryonic cardiac tissue (≈1–6 kPa).[60]

In previous literature, injectable hydrogels and 3D-printed constructs based on Gel and Alg hydrogels have been obtained by an external crosslinking method.[64-69] Alg/Gel hydrogels have been commonly described as interpenetrated (IPN) or semi-interpenetrated (semi-IPN) hydrogel networks, depending on the involved crosslinking mechanism. Semi-IPN hydrogels have been generally obtained by ionic crosslinking of Alg chains through calcium ions from $CaCl_2$ dissociation, with Gel physically entrapped in the Alg crosslinked network.[70-72] IPN hydrogels have also been obtained by combining ionic crosslinking of Alg, with additional Gel crosslinking

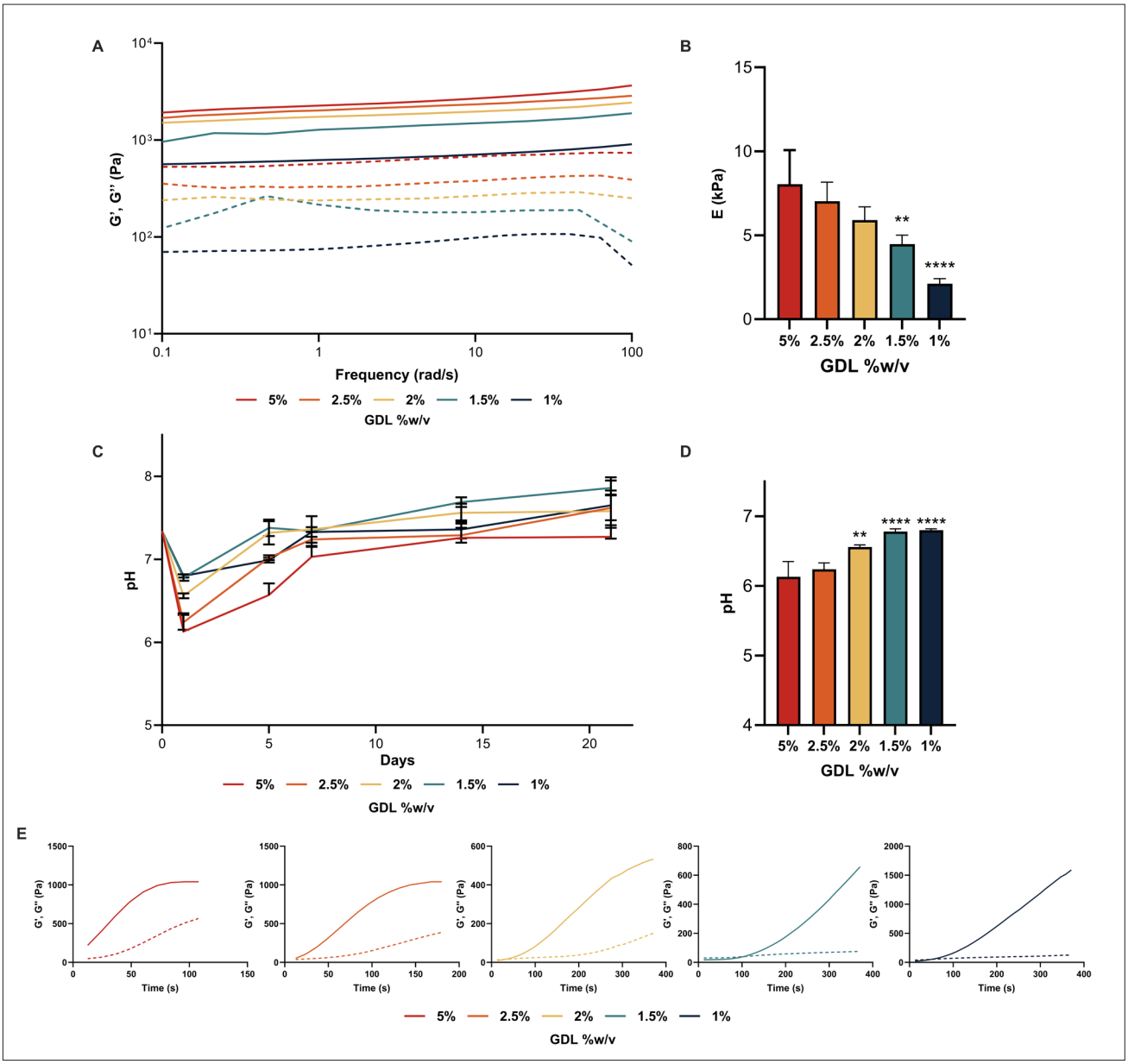

Figure 3. Rheological analyses and pH evaluation of ADA/Alg/Gel hydrogels. (A) Storage modulus (G′; continuous line) and loss modulus (G″; dotted line) of ADA/Alg_50/50_C6 with different concentrations of GDL (5% [w/v], red; 2.5% [w/v], orange; 2% [w/v], yellow; 1.5% [w/v], light blue; and 1% [w/v], blue) as a function of angular frequency (0.1 and 100 rad/s) at 37°C ($n = 3$). (B) Elastic modulus (E) of ADA/Alg_50/50_C6 with different concentrations of GDL (5% [w/v], red; 2.5% [w/v], orange; 2% [w/v], yellow; 1.5% [w/v], light blue; and 1% [w/v], blue) derived from frequency sweep test ($n = 3$). $^{**}p < 0.01$ and **** $p < 0.0001$ indicate statistically significant difference with 5% (w/v) GDL samples. (C–D) pH variation of ADA/Alg_50/50_C6 with different concentrations of GDL (5% [w/v], red; 2.5% [w/v], orange; 2% [w/v], yellow; 1.5% [w/v], light blue; and 1% [w/v], blue) measured after incubation at 37°C for 21 days (C) and after 24h (D) ($n = 3$). $^{**}p < 0.01$ and $^{****}p < 0.0001$ indicate statistically significant difference with 5% (w/v) GDL samples. (E) Time sweep analyses; evaluation of G′ (continuous line) and G″ (dotted line) as a function of time for ADA/Alg_50/50_C6 hydrogels with 5% (w/v) GDL (red), 2.5% (w/v) GDL (orange), 2% (w/v) GDL (yellow), 1.5% (w/v) GDL (light blue), and 1% (w/v) GDL (blue) at 37°C ($n = 2$). Abbreviations: Alg: Alginate; ADA: Alginate dialdehyde; GDL: D-(+)-glucono-1,5-lactone.

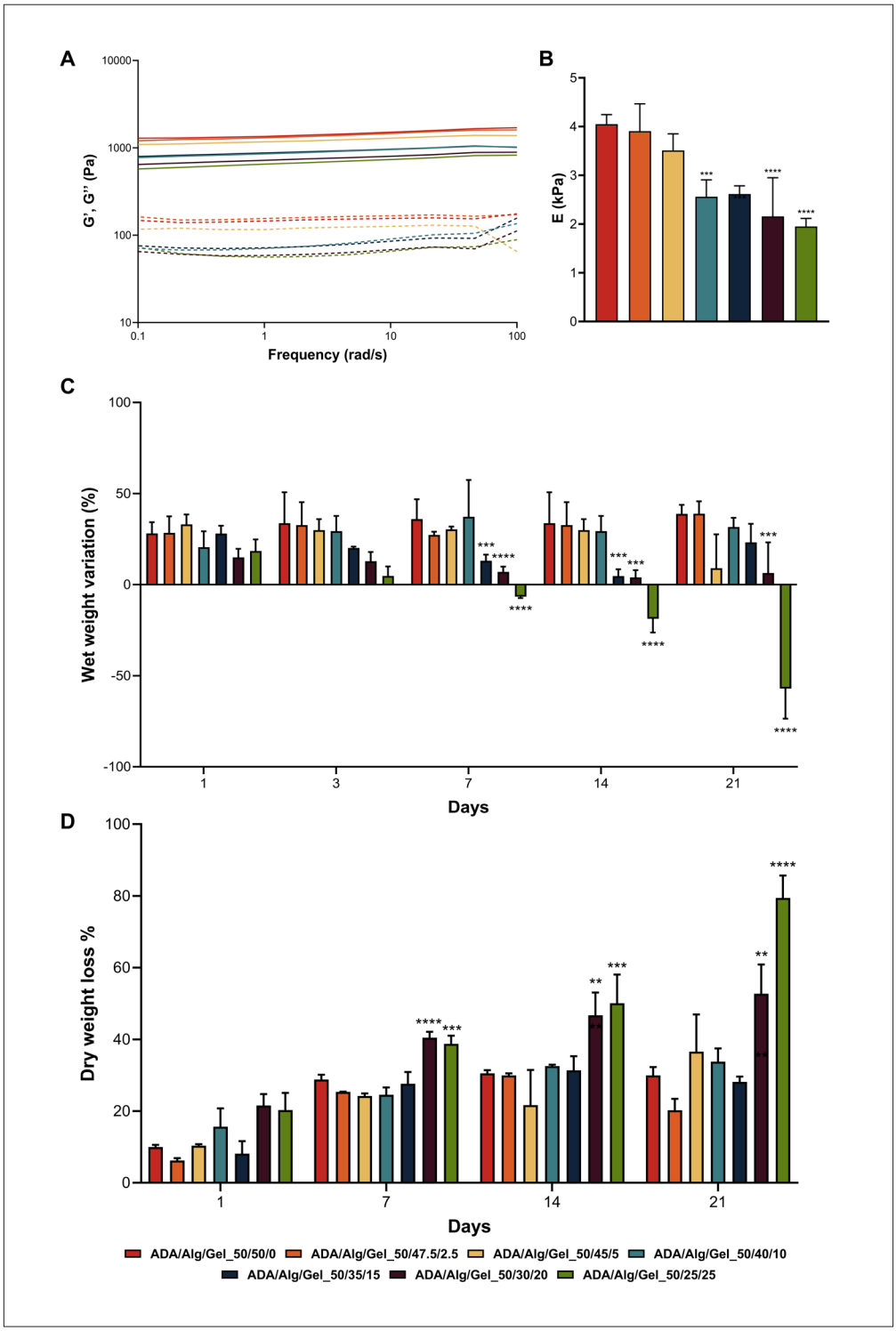

Figure 4. Rheological characterization and *in vitro* stability analysis of ADA/Alg/Gel hydrogels. (A) Storage modulus (G′; continuous line) and loss modulus (G″; dotted line) of ADA/Alg/Gel hydrogels as a function of angular frequency (0.1–100 rad/s) at 37°C (n = 3). (B) Elastic modulus (E) derived from frequency sweep test (n = 3). (C) Wet weight variation (%) of ADA-Alg/Gel hydrogels measured at 1, 3, 7, 14, and 21 days after incubation at 37°C (n = 3). (D) Dry weight loss (%) of ADA/Alg/Gel hydrogels measured at 1, 7, 14, and 21 days after incubation at 37°C (n = 3). In all graphs, the samples are ADA/Alg/Gel_50/50/0 (red), ADA/Alg/Gel_50/47.5/2.5 (orange), ADA/Alg/Gel_50/45/5 (yellow), ADA/Alg/Gel_50/40/10 (light blue), ADA/Alg/Gel_50/35/15 (blue), ADA/Alg/Gel_50/30/2 (purple), and ADA/Alg/Gel_50/25/25 (green). *$p < 0.05$, **$p < 0.01$, ***$p < 0.001$, and ****$p < 0.0001$ indicate statistically significant difference with ADA/Alg/Gel_50/50/0. Abbreviations: Alg: Alginate; ADA: Alginate dialdehyde; Gel: Gelatin.

triggered by an enzyme, such as transglutaminase,[73,74] or a chemical agent, such as carbodiimides,[65] glutaraldehyde,[66] or genipin.[67] In ADA/Alg/Gel-based hydrogels, chemical crosslinking between ADA and Gel could be achieved by Schiff base formation between ADA aldehyde groups and Gel amino groups. However, ADA/Gel hydrogels crosslinked by Schiff base reaction are weak and unstable due to the reversible nature of the formed chemical bonds and poor mechanical properties of Gel at physiological temperature. Therefore, ADA/Gel hydrogels are usually further crosslinked by external ionic crosslinking of ADA[68,69] and/or Gel crosslinking by transglutaminase.[73] To our knowledge, the herein investigated formulation of ADA/Alg/Gel hydrogels using only an internal ionic crosslinking mechanism has not been proposed so far. In this work, the rheological characterization of ADA/Alg/Gel hydrogels suggested the formation of a semi-INP network based on physically crosslinked ADA/Alg chains by calcium ions and non-crosslinked Gel chains. Indeed, the G′ of ADA/Alg/Gel hydrogels decreased proportionally with decreasing Alg content in the hydrogels. On the contrary, an increase in Gel amount did not increase the mechanical stiffness of hydrogels. To better understand ADA/Gel interactions, ATR-FTIR analysis and rheological characterization of only ADA/Gel hydrogels were conducted, selecting the highest ADA:Gel (~70:30) ratio investigated in this study for samples ADA/Alg/Gel_50/25/25. In the ADA/Gel FTIR spectrum (Figure S2A, Supporting Information), a broad peak at 1625 cm^{-1} was detected, associated with the overlapping of C=N vibration of Schiff base at 1620 cm^{-1} and amide I of uncrosslinked Gel at 1630 cm^{-1}.[41,75] Additionally, the shift of the amide II band from 1522 to 1540 cm^{-1}, characteristic of Gel, along with the complete absence of the 1740 cm^{-1} band, associated with the carbonyl groups of ADA in the ADA/Gel spectrum, indicated the possible involvement of these groups in Schiff bond formation.[76] Nonetheless, further rheological characterization of ADA/Gel hydrogels (Figure S2B, Supporting Information) suggested that these interactions were not sufficient to form a fully crosslinked chemical network at the investigated concentrations. A possible explanation of these contrasting results could be associated with the hypothesis of having Gel chains linked to ADA through Schiff base interactions (ADA-modified Gel chains) without forming a fully crosslinked chemical network. Hydrogel formation via Schiff base reactions depends on ADA oxidation degree and MW, and the molar ratio between ADA aldehyde groups and Gel amino moieties.[68,77] Results from this work are in agreement with previous literature studies on ADA/Gel hydrogels based on ADA with a similar oxidation degree of around 25%. In those studies, fully formed ADA/Gel hydrogels were only obtained through an additional ionic crosslinking strategy.[41,73,77] Therefore, previous findings further support our hypothesis that ADA/Alg/Gel hydrogels with internal ionic crosslinking are based on a semi-IPN network.

Future work will focus on optimizing ADA production to achieve oxidation degrees and MW suitable to form fully crosslinked ADA/Gel Schiff-base hydrogels, investigating the development of fully interpenetrated time-dependent ADA/Alg/Gel systems. In this regard, ADA with different oxidation degrees will be tested for efficient crosslinking of Gel chains. Additionally, the amination reaction between ADA and Gel (through sodium borohydride or sodium cyanoborohydride) could further improve network stability but would require a careful evaluation of its implementation to avoid cell cytotoxicity.[78]

3.3.2. In vitro stability studies

Hydrogel stability was studied by evaluating wet and dry weight changes upon incubation in PBS for 21 days. Both wet and dry weight loss were monitored to obtain comprehensive insights into hydrogel stability and degradation rate. Wet weight assessment provides immediate information on the total mass of the hydrogel, allowing the evaluation of swelling behavior and hydration dynamics. In contrast, dry weight assessment enables precise tracking of material degradation, offering a clearer understanding of the hydrogel's long-term stability and structural integrity.

Wet weight variation percentage over time is reported in Figure 4C. ADA/Alg/Gel_50/50/0 hydrogel displayed an increase in wet weight after 24 h of incubation, reaching an average wet weight variation percentage of 21 ± 9%, which then remained constant for up to 21 days. The introduction of Gel induced composition-dependent variations in the wet weight profile. Samples with the lowest Gel content (ADA/Alg/Gel_50/47.5/2.5, ADA/Alg/Gel_50/45/5, and ADA/Alg/Gel_50/40/10) exhibited a behavior similar to ADA/Alg/Gel_50/50/0. Hydrogels with a higher Gel content (ADA/Alg/Gel_50/35/15 and ADA/Alg/Gel_50/30/20) reached a lower wet variation percentage (13 ± 9% and 7 ± 3%, respectively) compared to ADA/Alg/Gel_50/50/0 after seven days ($p < 0.0002$ and $p < 0.0001$, respectively). Finally, the hydrogel composition with the highest Gel content (ADA/Alg/Gel_50/25/25) exhibited a decrease in wet weight over time, with a negative wet weight variation percentage after seven days of incubation in PBS. This behavior suggested that the samples released polymeric components while absorbing PBS, with prevalent dissolution over swelling starting from day 7 of incubation in PBS.

The dry weight loss on day 21 of incubation in PBS is reported in Figure 4D. After seven days, ADA/Alg/Gel_50/50/0 displayed a 30 ± 1% dry weight loss, which remained constant over time. Hydrogels with the lowest Gel content (ADA/Alg/Gel_50/47.5/2.5, ADA/Alg/Gel_50/45/5, ADA/Alg/Gel_50/40/10, and ADA/Alg/Gel_50/35/15) behaved similarly to ADA/Alg/Gel_50/50/0, with no statistically significant differences. On the contrary, hydrogels with the highest Gel contents (ADA/Alg/Gel_50/30/20 and ADA/Alg/Gel_50/25/25) presented significantly higher dry weight loss compared to ADA/Alg/Gel_50/50/0 at all the evaluated time points ($p < 0.0021$ on days 1, 14, and 21 and $p < 0.0001$ on day 7 for ADA/Alg/Gel_50/30/20; $p < 0.0332$ on day 1, $p < 0.0002$ on days 7 and 14, and $p < 0.0001$ on day 21 for ADA/Alg/Gel_50/25/25). Moreover, ADA/Alg/Gel_50/30/20 and ADA/Alg/Gel_50/25/25 dry weight loss increased over time, reaching 53 ± 8% for ADA/Alg/Gel_50/30/20 and 80 ± 6% for ADA/Alg/Gel_50/25/25 after 21 days.

Biodegradability is a critical requirement in TE applications, both for regenerative applications and *in vitro* models. Dissolution of ionically crosslinked Alg-based hydrogels in the aqueous environment is regulated by the exchange between divalent calcium ions and monovalent cations (e.g., Na^+), inducing calcium ion release into the surrounding media.[10,11,37] The dissolution process is usually long-lasting and depends on Alg concentration and degree of crosslinking, requiring at least a month to achieve significant initial weight loss.[11,57] The introduction of ADA within the matrix has the advantage of increasing the dissolution rate due to the higher susceptibility of ADA to hydrolytic scission and β-elimination at physiological pH.[58,79] Moreover, for prospective *in vivo* applications, ADA with MW lower than 50 kDa (like the one produced in this work) can be removed from the human body by kidney clearance.[34,57] In our work, ADA/Alg/Gel featured a tunable degradation profile depending on the Gel concentration selected, providing a versatile hydrogel platform for TE applications. The dependence of hydrogel stability on Gel content is probably associated with the release of Gel from the ADA/Alg/Gel semi-IPN network at 37°C (with Gel in sol state). Specifically, hydrogels with the highest Gel content (20% and 25% wt.; Table 2) exhibited a dry weight loss exceeding the initial Gel percentage, namely 53% and 80% wt., respectively, after 21 days of incubation in PBS. This behavior suggests the release of Gel linked to ADA chains (i.e., ADA-modified Gel chains), which were not integrated into a broader chemical network. Therefore, the release of such ADA-modified Gel chains could explain the higher dry weight loss observed. In addition, decreased stability of ADA/Alg/Gel systems could also be associated with the reduction of the total Alg content (from 50 to 25% [w/w]) within the system proportional to the increment of Gel (from 0 to 25% [w/w]). In the ADA/Alg/Gel semi-IPN network, Alg is the main component that interacts with calcium ions; hence, the reduction of this component could also lead to decreased hydrogel stability. The presence of Gel in the ADA/Alg/Gel network is also expected to enhance the enzymatic degradation of the hydrogel, though not tested in this work. Thus, forthcoming investigations should involve *in vitro* degradation studies in the presence of relevant enzymes (e.g., collagenase).

3.3.3. Printability evaluation of Alg/ADA/Gel bioinks

Based on the rheological and stability properties of ADA/Alg/Gel samples, three compositions were selected to be investigated as hydrogel inks for 3D microextrusion printing: ADA/Alg/Gel_50/50/0 with no Gel in the network; ADA/Alg/Gel_50/40/10 having intermediate Gel concentration; and ADA/Alg/Gel_50/25/25 with the highest Gel content. The three compositions were selected to evaluate the printability of Alg/ADA/Gel bioinks as a platform with tunable degradability, stiffness, and cell adhesive properties. Due to the time-dependance of the internal crosslinking mechanism, printability was investigated over time through viscosity tests and microscopy analyses of 3D-printed structures.

Figure 5A–C presents the variations in apparent viscosity over time, studied by shear sweep tests. Regarding the composition without Gel (ADA/Alg/Gel_50/50/0), a Newtonian region was detected immediately after hydrogel preparation (i.e., t = 2 min; time required to load the sample on the rheometer and start the measurement), corresponding to a constant viscosity at low shear rates (< 1 rad/s). Conversely, a shear-thinning behavior was observed for shear rates higher than 1 rad/s.[80,81] This behavior is typically displayed by non-crosslinked Alg solutions or hydrogels.[70,80] After 10 min, ADA/Alg/Gel_50/50/0 displayed a shear-thinning behavior at all the shear rates investigated, and this trend remained constant over time. The other two hydrogel compositions containing Gel exhibited a shear-thinning behavior for all the time points investigated, without Newtonian behavior even immediately after hydrogel preparation.

Thereafter, 2D grid structures (15 × 15 mm^2) with a strand spacing of 2.5 mm were then printed at selected time points, and variations in average fiber dimension, spreading ratio (S), and printability index (Pr) were evaluated as a function of time.

All the compositions displayed a variation in fiber diameter as a function of time (Figure 5D–F). ADA/Alg/Gel_50/50/0 bioinks could be printed at the shortest time points (i.e., 10 and 20 min), resulting in well-defined 2D

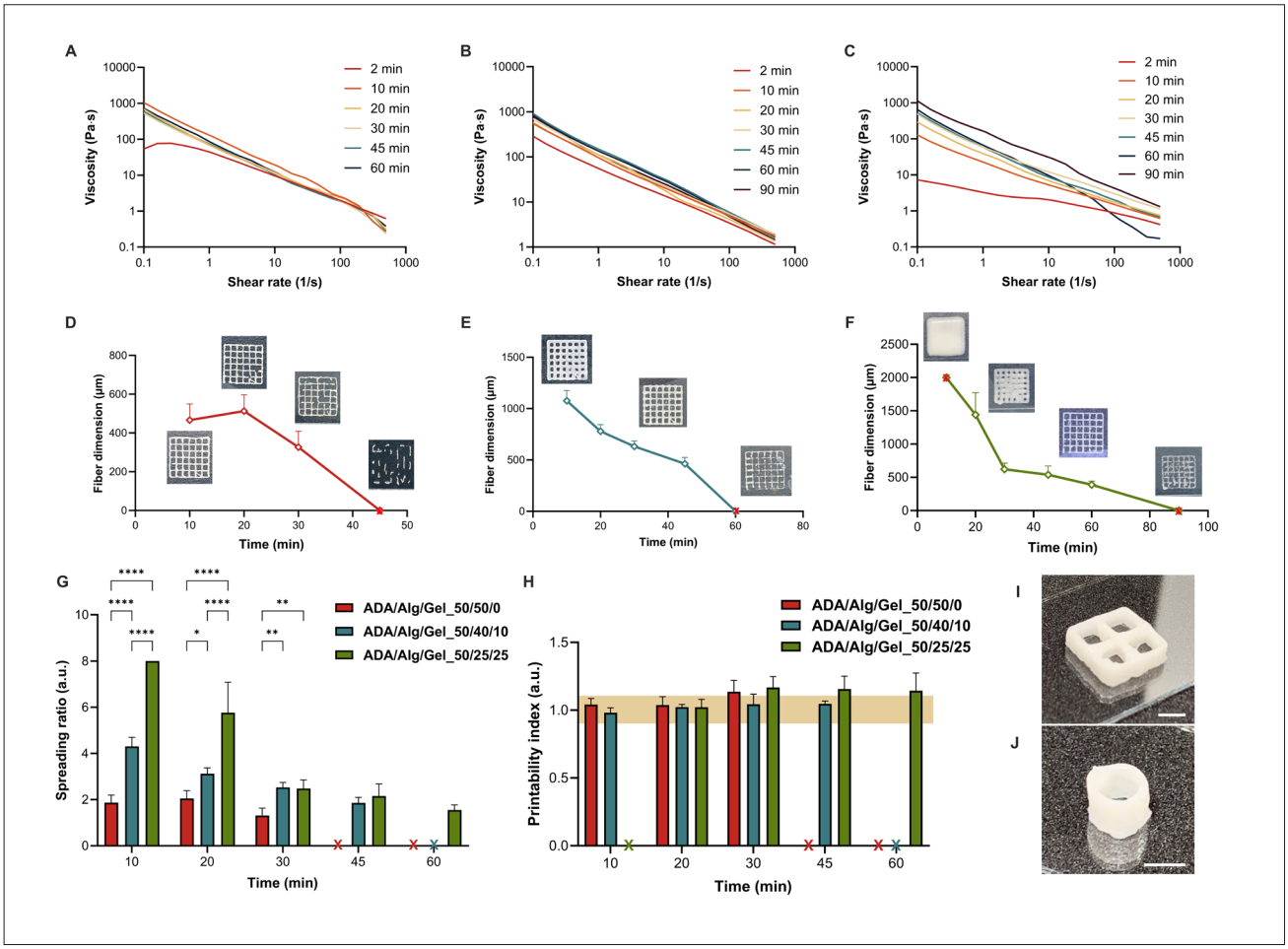

Figure 5. Printability characterization of ADA/Alg/Gel hydrogels (A–C) Viscosity curve as a function of the shear rate for ADA/Alg/Gel_50/50/0 (A), ADA/Alg/Gel_50/40/10 (B), and ADA/Alg/Gel_50/25/25 (C) measured at 2, 10, 20, 30, 45, 60, and 90 min after hydrogel preparation. (D–F) Variations in fiber diameter over time for ADA/Alg/Gel_50/50/0 (D), ADA/Alg/Gel_50/40/10 (E), and ADA/Alg/Gel_50/25/25 (F) (n = 10). (G) Spreading ratio over time for ADA/Alg/Gel_50/50/0 (red), ADA/Alg/Gel_50/40/10 (light blue), and ADA/Alg/Gel_50/25/25 (green) (n = 10). *p < 0.05, **p < 0.01, and ****p <0.0001 indicate statistically significant differences with ADA/Alg/Gel_50/50/0. (H) Printability index over time for ADA/Alg/Gel_50/50/0 (red), ADA/Alg/Gel_50/40/10 (light blue), and ADA/Alg/Gel_50/25/25 (green) (n = 10). (I and J) Optical images of self-standing (I) 3D square samples (10 × 10 mm^2; five layers) and (J) hollow 3D cylindrical structures (diameter, ∅: 3 mm; 10 layers). Scale bars: 5 mm. Abbreviations: Alg: Alginate; ADA: Alginate dialdehyde; Gel: Gelatin.

grid structures with an average filament diameter of 465 ± 80 µm at 10 min and 510.0 ± 85 µm at 20 min. After 30 min, the average fiber diameter decreased to 330 ± 80 µm, closer to the ideal value of 250 µm (i.e., similar to the nozzle diameter); however, inhomogeneities were observed (Figure 5D). Finally, after 45 min, a continuous grid structure could not be printed due to complete hydrogel crosslinking. The samples containing Gel displayed a significantly higher fiber size immediately after printing due to bioink overflow and delayed crosslinking onset. Particularly, well-defined grid structures with spaced individual filaments of ADA/Alg/Gel_50/40/10 could only be printed 20 min after hydrogel preparation (Figure 5E), while 30 min was required for ADA/Alg/Gel_50/25/25 (Figure 5F). The smallest fiber diameter was achieved after 45 min for ADA/Alg/Gel_50/40/10 (464 ± 60 µm) and after 60 min for ADA/Alg/Gel_50/25/25 (390 ± 55 µm). As for ADA/Alg/Gel_50/50/0 hydrogel, continuous grid structures could not be obtained even after longer durations, i.e., 60 min for ADA/Alg/Gel_50/40/10 hydrogel and 90 min for ADA/Alg/Gel_50/25/25 hydrogel.

The ADA/Alg/Gel samples demonstrated a similar trend for variations in spreading ratio over time as fiber dimensions (Figure 5G). For ADA/Alg/Gel_50/50/0 hydrogel, a spreading ratio between 1.3 and 2.05 was obtained between 10 and 30 min. The spreading ratio of

Gel containing hydrogel was significantly higher than that for ADA/Alg/Gel_50/50/0 at all the evaluated time points. At longer times, well-defined 3D structures could not be printed, and both compositions exhibited spreading ratios above 3 (4.3 ± 0.5 for ADA/Alg/Gel_50/40/10 after 10 min; 8 and 5.8 ± 1.3 for ADA/Alg/Gel_50/25/25 after 10 and 20 min, respectively). For ADA/Alg/Gel_50/40/10 hydrogel, the average spreading ratio decreased from 3.1 ± 0.3 to 1.8 ± 0.2 between 20 and 45 min (i.e., 3.1 ± 0.3, 2.5 ± 0.2, and 1.8 ± 0.2 after 20, 30, and 45 min); while the spreading ratio for ADA/Alg/Gel_50/25/25 decreased from 2.5 to 1.5 between 30 and 60 min (2.5 ± 0.4, 2.1 ± 0.5, and 1.5 ± 0.2 after 30, 45, and 60 min).

Finally, the Pr was measured to evaluate possible under- or over-gelation phenomena of the inks (Figure 5H). At conditions allowing the printing of continuous filaments and well-defined grid structures (10–30 min for ADA/Alg/Gel_50/50/0; 10–45 min for ADA/Alg/Gel_50/40/10; and 20–60 min for ADA/Alg/Gel_50/25/25), the three compositions exhibited a Pr between 0.9 and 1.1, indicating the formation of square-shaped pores[82] (Pr = 1, indicates perfectly square-shaped pores), with no statistically significant differences among the samples with/without Gel (Figure 5H).

Microextrusion printing of Alg-based hydrogel was previously investigated using external ionic crosslinking with calcium ions and supporting baths. The process requires optimization of the hydrogel ink and supporting bath to print complex 3D structures.[20] Moreover, external gelation is inherently associated with the formation of non-homogeneous filaments with a highly crosslinked surface, causing potential detrimental effects on nutrient exchange.[24,25] Additionally, for drug delivery applications, the use of a crosslinking solution can lead to a fast release of the encapsulated molecules during the gelation phase.[27] To overcome these drawbacks, internal ionic crosslinking represents a promising approach for the development of Alg-based ink. Only a few studies have investigated internal gelation for Alg-based inks, highlighting its ability to generate homogeneous scaffolds without the need for post-crosslinking strategies or supporting baths. Specifically, Remaggi et al. investigated the application of internally crosslinked Alg inks for drug delivery for breast cancer treatment, using printing conditions (i.e., curing time of three days at 2°C) not suitable for cell bioprinting.[27] Sardelli et al. explored Alg ink printability via internal gelation, evaluating material properties and fiber printability over 24 h, but without biological characterization. To our knowledge, only three studies by the same group developed a bioink for cell bioprinting based on an internally crosslinked Alg hydrogel added with porcine liver-derived decellularized ECM to design *in vitro* models of hepatic tissue.[31,32] In these reports, the authors demonstrated the hydrogel ability to support mid/long-term cultures of human liver cancer cells (HepG2).[31-33] In this work, we investigated the bioprinting of ADA/Alg/Gel hydrogels, exploiting an internal crosslinking mechanism to fabricate biodegradable, biocompatible, and self-standing ADA-based 3D-printed scaffolds for prospective cardiac TE. Considering the time-dependent nature of the internal crosslinking mechanism,[28] an in-depth investigation of ADA/Alg/Gel printability was performed, evaluating viscosity and shape fidelity (i.e., spreading ratio and Pr) over time. Specifically, printability was optimized within short time intervals (i.e., below 90 min), as long printing times can severely decrease the viability of cells embedded in the bioink.[83,84] ADA/Alg/Gel_50/50/0, ADA/Alg/Gel_50/40/10, and ADA/Alg/Gel_50/25/25 hydrogels demonstrated suitable printability times of 10, 20, and 30 min, respectively. Given the internal gelation mechanism exploited in the study, the printability of the hydrogels is attributed to the gradual pH-triggered release of calcium ions, leading to time-dependent crosslinking, as evidenced by printability studies. The delay in printability observed for the samples with higher Gel content was probably related to the steric hindrance of uncrosslinked Gel within the semi-IPN network, slowing down the crosslinking process.[39] Indeed, the presence of additives in internally crosslinked Alg-based hydrogels significantly affected their rheological behavior, including gelation.[33,85,86] However, it is not possible to exclude other factors that might concur to determine such delay.

Finally, as a proof-of-concept, Figure 5I and J features 3D structures based on ADA/Alg/Gel_50/25/25, printed after 60 min from hydrogel components, having a grid (1.25 mm height, five layers; Figure 5I) and cylindrical geometry (2.25 mm height, 10 layers; Figure 5J). Hence, ADA/Alg/Gel hydrogels can be used for printing self-standing 3D structures with various shapes by internal crosslinking with no need for a supporting bath. Unlike previous works,[32] multilayer structures were developed without the need for curing or post-processing of the bioink.

3.3.4. Bioink in vitro cytocompatibility and printability

In vitro indirect cell cytocompatibility tests were carried out to investigate the potential cytotoxic effect of eluates from ADA/Alg/Gel_50/50/0, ADA/Alg/Gel_50/40/10, and ADA/Alg/Gel_50/25/25 hydrogels by *in vitro* culture of AHCFs for 24 h in the presence of eluates, following ISO 10993. Results indicated increasing cell viability for hydrogels with increasing Gel content (Figure 6A). Indeed, AHCFs cultured with eluates from ADA/Alg/Gel_50/50/0,

ADA/Alg/Gel_50/40/10, and ADA/Alg/Gel_50/25/25 hydrogels reported 70% ($p < 0.0021$), 83% ($p < 0.0332$), and 87% cell viability compared to control AHCFs, respectively. Cell cytotoxicity assay (Figure 6B) confirmed low (< 6% in ADA/Alg/Gel_50/50/0 and ADA/Alg/Gel_50/40/10) or no cytotoxic effects (in ADA/Alg/Gel_50/25/25) for hydrogel eluates with AHCFs, demonstrating hydrogel cytocompatibility ($p < 0.0001$).

Then, bioprinting of AHCFs embedded into ADA/Alg/Gel_50/50/0, ADA/Alg/Gel_50/40/10, and ADA/Alg/Gel_50/25/25 hydrogels was investigated. Live/dead assay performed 1 h post-printing displayed high cell viability for all samples (Figure 6C). However, after 24 h post-printing (Figure 6D and E), the viability of AHCFs embedded into ADA/Alg/Gel_50/50/0, ADA/Alg/Gel_50/40/10, and ADA/Alg/Gel_50/25/25 hydrogel was 45, 50, and 92% ($p < 0.0001$ compared to red-stained dead cells), respectively. To further validate the developed bioink suitability for cardiac TE, the bioprinting of H9C2 cells embedded in ADA/Alg/Gel_50/25/25 hydrogels was examined. Live/dead assays demonstrated excellent cell viability 1 h after printing (Figure 6F) and indicated high viability 24 h post-printing (Figure 6F and G), with 83% of viable cells ($p < 0.0001$ compared to red-stained dead cells).

In this work, Gel was added within the system to overcome one of the main limitations of Alg and ADA-based hydrogels, i.e., the lack of cell adhesive moieties. Moreover, as reported in previous studies, ADA-based hydrogels may elicit cell cytotoxicity due to oxidative stresses induced by the presence of free aldehyde groups.[75,87] Specifically, ADA-based hydrogels can affect the viability of both primary human fibroblasts and endothelial cells by depleting cellular thiols, increasing reactive oxygen species (ROS) generation.[75] The combination of ADA with Gel reportedly reduces ADA cytotoxicity due to aldehyde group shielding by Gel primary amine groups via Schiff base formation.[75,87] In this work, low cell viability within ADA/Alg/Gel_50/50/0 and ADA/Alg/Gel_50/40/10 hydrogel at 24 h post-printing was probably caused by the combination of the lack of cell adhesion moieties and the cytotoxic effects of aldehyde groups in the hydrogel. Indeed, in the sample without Gel, ADA aldehyde groups are free to interact with cellular components, inducing cytotoxicity. Cell viability results indicated that the addition of 10% Gel was not sufficient to improve the cytocompatibility of the system, suggesting the persistence of a high number of free aldehyde groups within the matrix, combined with insufficient addition of cell adhesive groups. On the contrary, increasing Gel concentration to 25% (w/w) (ADA/Alg/Gel_50/25/25) drastically improved cell viability at 24 h post-printing. The improved cell viability could be associated with an increase in cell adhesive moieties present within the hydrogel matrix. Moreover, as ADA content was kept constant in all the formulations, increasing the Gel content could be directly correlated with a higher number of Gel primary amine groups that can interact with free aldehyde groups in ADA, decreasing their cytotoxicity. As a proof-of- concept, we demonstrated the bioink suitability for prospective cardiac TE by bioprinting H9C2 cells in ADA/Alg/Gel_50/25/25 hydrogels, with excellent cell viability at 1 and 24 h post-printing.

In this study, a bioink supporting cardiac cell printing and initial adhesion was designed based on time-dependent internal ionic crosslinking. Future studies will evaluate longer culture times for bioinks cellularized with AHCFs, human induced pluripotent stem cells derived cardiomyocytes. and their co-cultures to assess the effect of hydrogel on cell proliferation, maturation, and matrix remodeling with the deposition of new ECM. New knowledge will be obtained for the *in vitro* engineering of 3D cardiac tissue with controlled and reproducible structure by bioprinting, which can be exploited as *in vitro* cardiac tissue models or cardiac patches.

4. Conclusion

In this study, we investigated, for the first time, the development of novel ADA/Alg/Gel-based bioinks, exploiting an internal crosslinking mechanism method to achieve self-standing 3D scaffolds for prospective applications in *in vitro* cardiac TE. Polymer concentration, as well as $CaCO_3$ and GDL content, were tuned to obtain 3D-printed constructs with a faster degradation rate (imparted by ADA and Gel) and the ability to support cell adhesion (due to Gel adhesive moieties). Printability studies revealed that all ADA/Alg/Gel formulations demonstrated time-dependent shear-thinning behavior suitable for 3D bioprinting. This behavior is attributed to the gradual pH-triggered release of calcium ions over time and is influenced by Gel content. Notably, self-standing and multilayer 3D structures could be printed, exploiting internal gelation without the addition of any post-crosslinking agents or supporting baths. *In vitro* biological tests confirmed that the bioinks and selected printing process parameters preserved cell viability. Hydrogel composition with the highest Gel content was able to support the viability of AHCFs and H9C2 embedded in the hydrogels, at 24 h post-printing.

Such innovative bioinks are promising in the field of soft TE, particularly for prospective cardiac TE, due to the cardiac tissue-like stiffness of the inks and their ability

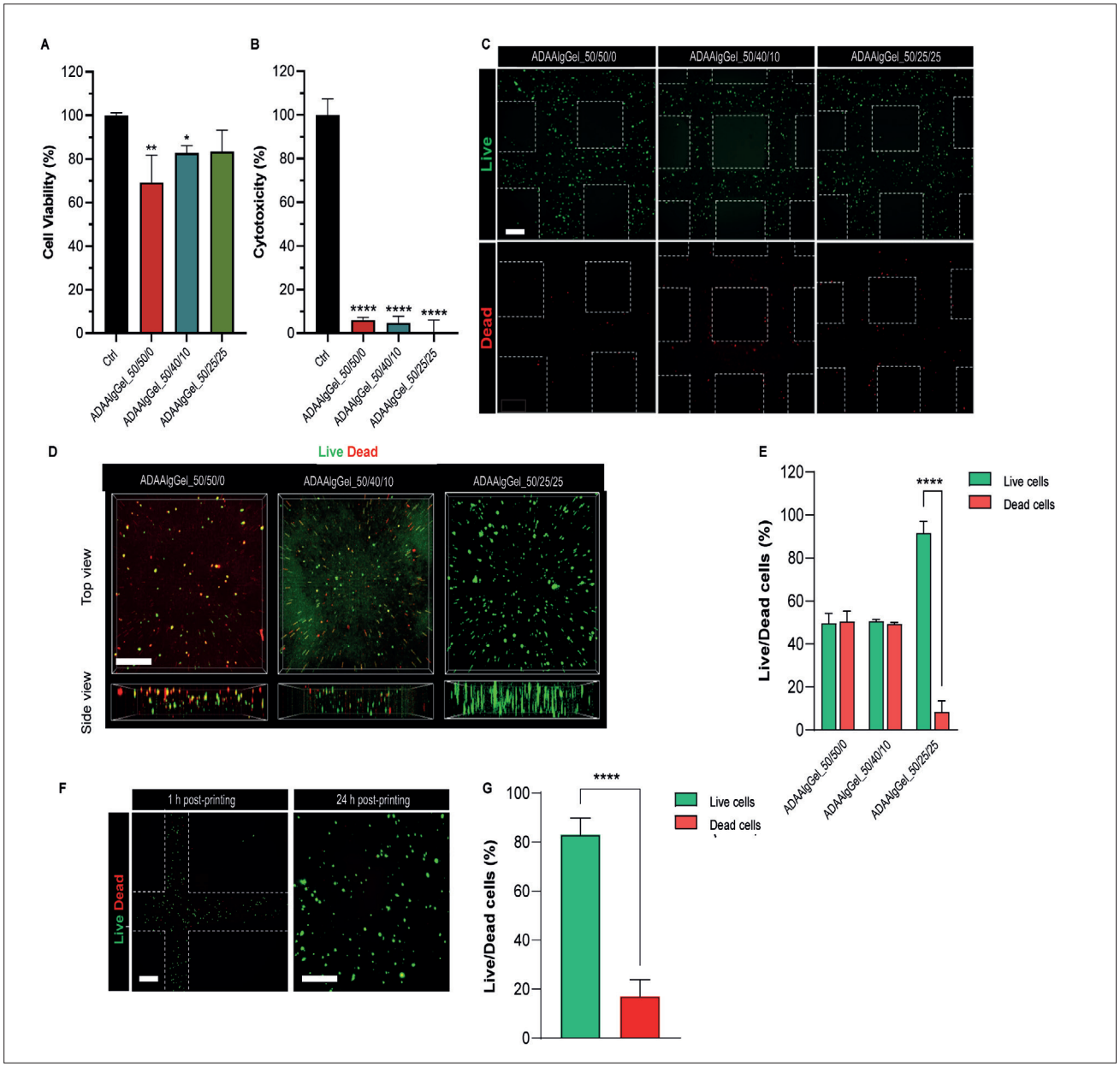

Figure 6. *In vitro* characterization of ADA/Alg/Gel hydrogels (A and B) Viability (A) and toxicity (B) studies ($n = 3$) of ADA/Alg/Gel_50/50/0 (red), ADA/Alg/Gel_50/40/10 (blue), and ADA/Alg/Gel_50/25/25 (green); for viability studies (A), the control group consists of AHCFs cultured on tissue culture plastic with untreated media; for toxicity studies (B), the control group consists of AHCFs cultured on tissue culture plastic with 100% of cell death induced by CytoTox-ONE™ lysis solution (grey). $^{*}p < 0.05$, $^{**}p < 0.01$, and $^{****}p < 0.0001$ indicate statistically significant differences between the compositions and the control group. (C and D) Live/dead assay performed on AHCF-laden ADA/Alg/Gel_50/50/0, ADA/Alg/Gel_50/40/10, and ADA/Alg/Gel_50/25/25 hydrogels at 1 h (C) and 24 h (D) after printing. Scale bars: 100 μm (C) and 500 μm (D). (E) Quantification of live (green) and dead (red) AHCFs at 24 h after printing. $^{****}p < 0.0001$ indicates a statistically significant difference between the live and dead cells for ADA/Alg/Gel_50/25/25 ($n = 9$). (F) Live/dead assay performed on H9C2-laden ADA/Alg/Gel_50/25/25 hydrogels after 1 and 24 h. Scale bars: 100 μm (1h, left image) 500 μm (24h, right image). (G) Quantification of live (green) and dead (red) H9C2 at 24 h after printing. $^{****}p < 0.0001$ indicates a statistically significant difference between the live and dead cells for ADA/Alg/Gel_50/25/25 ($n = 9$). Abbreviations: AHCF: Adult human cardiac fibroblast; Alg: Alginate; ADA: Alginate dialdehyde; Gel: Gelatin.

to support AHCF and H9C2 viability. In conclusion, this work provides valuable insights toward overcoming the limitations associated with traditional Alg-based hydrogel bioinks.

Acknowledgments

Not applicable.

Funding

This work was supported by the European Research Council (ERC) under the European Union's Horizon 2020 research and innovation program (BIORECAR, grant agreement number 772168).

Conflict of interest

Elena Marcello serves as the Editorial Board Member of the journal, but was not in any way involved in the editorial and peer-review process conducted for this paper, directly or indirectly. Other authors declare they have no competing interests.

Author contributions

Conceptualization: Elena Marcello, Valeria Chiono
Funding acquisition: Valeria Chiono
Investigation: Giovanni Paolo Stola, Camilla Paoletti, Letizia Nicoletti, Elena Marcello, Geo Paul, Claudio Cassino, Leonardo Marchese
Writing – original draft: Elena Marcello, Giovanni Paolo Stola, Camilla Paoletti
Writing – review & editing: Elena Marcello, Valeria Chiono

Ethics approval and consent to participate

Not applicable.

Consent for publication

Not applicable.

Availability of data

Data are available from the corresponding author upon reasonable request.

References

1. Fatimi A, Okoro OV, Podstawczyk D, Siminska-Stanny J, Shavandi A. Natural hydrogel-based bio-inks for 3D bioprinting in tissue engineering: a review. *Gels*. 2022;8(3):179. doi: 10.3390/gels8030179
2. Ramiah P, du Toit LC, Choonara YE, Kondiah PPD, Pillay V. Hydrogel-based bioinks for 3D bioprinting in tissue regeneration. *Front Mater*. 2020;7:506968. doi: 10.3389/FMATS.2020.00076/BIBTEX
3. Taneja H, Salodkar SM, Singh Parmar A, Chaudhary S. Hydrogel based 3D printing: bio ink for tissue engineering. *J Mol Liq*. 2022;367:120390. doi: 10.1016/J.MOLLIQ.2022.120390
4. Wissing TB, Bonito V, Bouten CVC, Smits AIPM. Biomaterial-driven *in situ* cardiovascular tissue engineering—a multi-disciplinary perspective. *NPJ Regen Med*. 2017;2(1):1-20. doi: 10.1038/s41536-017-0023-2
5. Mei X, Cheng K. Recent development in therapeutic cardiac patches. *Front Cardiovasc Med*. 2020;7:610364. doi: 10.3389/fcvm.2020.610364
6. Testore D, Zoso A, Kortaberria G, Sangermano M, Chiono V. Electroconductive photo-curable PEGDA-Gelatin/PEDOT: PSS hydrogels for prospective cardiac tissue engineering application. *Front Bioeng Biotechnol*. 2022;10:897575. doi: 10.3389/fbioe.2022.897575
7. Neuhaus W, Reininger-Gutmann B, Rinner B, et al. The rise of three rs centres and platforms in Europe*. *Altern Lab Anim*. 2022;50(2):90-120. doi: 10.1177/02611929221099165
8. Panwar A, Tan LP. Current status of bioinks for micro-extrusion-based 3D bioprinting. *Molecules*. 2016;21(6):685. doi: 10.3390/molecules21060685
9. He Y, Yang F, Zhao H, Gao Q, Xia B, Fu J. Research on the printability of hydrogels in 3D bioprinting. *Sci Rep*. 2016;6(1):1-13. doi: 10.1038/srep29977
10. Sun J, Tan H. Alginate-based biomaterials for regenerative medicine applications. *Materials*. 2013;6(4):1285-1309. doi: 10.3390/ma6041285
11. Lee KY, Mooney DJ. Alginate: properties and biomedical applications. *Prog Polym Sci (Oxford)*. 2012;37(1):106-126. doi: 10.1016/j.progpolymsci.2011.06.003
12. Lee RJ, Hinson A, Bauernschmitt R, et al. The feasibility and safety of Algisyl-LVR™ as a method of left ventricular augmentation in patients with dilated cardiomyopathy: initial first in man clinical results. *Int J Cardiol*. 2015;199:18-24. doi: 10.1016/j.ijcard.2015.06.111
13. Ruvinov E, Cohen S. Alginate biomaterial for the treatment of myocardial infarction: progress, translational strategies, and clinical outlook. From ocean algae to patient bedside. *Adv Drug Deliv Rev*. 2016;96:54-76. doi: 10.1016/j.addr.2015.04.021
14. Choy JS, Leng S, Acevedo-Bolton G, et al. Efficacy of intramyocardial injection of Algisyl-LVR for the

treatment of ischemic heart failure in swine. *Int J Cardiol*. 2018;255:129-135.
doi: 10.1016/j.ijcard.2017.09.179

15. Cao L, Lu W, Mata A, Nishinari K, Fang Y. Egg-box model-based gelation of alginate and pectin: a review. *Carbohydr Polym*. 2020;242:116389.
doi: 10.1016/j.carbpol.2020.116389

16. Hu C, Lu W, Mata A, Nishinari K, Fang Y. Ions-induced gelation of alginate: mechanisms and applications. *Int J Biol Macromol*. 2021;177:578-588.
doi: 10.1016/j.ijbiomac.2021.02.086

17. Paques JP. Alginate nanospheres prepared by internal or external gelation with nanoparticles. In: *Microencapsulation and Microspheres for Food Applications*. Cambridge, USA: Academic Press; 2015:39-55.
doi: 10.1016/B978-0-12-800350-3.00004-2

18. Chan LW, Lee HY, Heng PWS. Mechanisms of external and internal gelation and their impact on the functions of alginate as a coat and delivery system. *Carbohydr Polym*. 2006;63(2):176-187.
doi: 10.1016/j.carbpol.2005.07.033

19. Hinton TJ, Jallerat Q, Palchesko RN, et al. Three-dimensional printing of complex biological structures by freeform reversible embedding of suspended hydrogels. *Sci Adv*. 2015;1(9):e1500758.
doi: 10.1126/sciadv.1500758

20. Mirdamadi E, Tashman JW, Shiwarski DJ, Palchesko RN, Feinberg AW. FRESH 3D bioprinting a full-size model of the human heart. *ACS Biomater Sci Eng*. 2020;6(11):6453-6459.
doi: 10.1021/acsbiomaterials.0c01133

21. Mirdamadi E, Muselimyan N, Koti P, Asfour H, Sarvazyan N. Agarose slurry as a support medium for bioprinting and culturing freestanding cell-laden hydrogel constructs. *3D Print Addit Manuf*. 2019;6(3):158-164.
doi: 10.1089/3dp.2018.0175

22. Hazur J, Detsch R, Karakaya E, et al. Improving alginate printability for biofabrication: establishment of a universal and homogeneous pre-crosslinking technique. *Biofabrication*. 2020;12(4):045004.
doi: 10.1088/1758-5090/ab98e5

23. Girón-Hernández J, Gentile P, Benlloch-Tinoco M. Impact of heterogeneously crosslinked calcium alginate networks on the encapsulation of β-carotene-loaded beads. *Carbohydr Polym*. 2021;271:118429.
doi: 10.1016/j.carbpol.2021.118429

24. Baker BM, Chen CS. Deconstructing the third dimension-how 3D culture microenvironments alter cellular cues. *J Cell Sci*. 2012;125(13):3015-3024.
doi: 10.1242/jcs.079509

25. Marchioli G, Van Gurp L, Van Krieken PP, et al. Fabrication of three-dimensional bioplotted hydrogel scaffolds for islets of Langerhans transplantation. *Biofabrication*. 2015;7(2).
doi: 10.1088/1758-5090/7/2/025009

26. Lee A, Hudson AR, Shiwarski DJ, et al. 3D bioprinting of collagen to rebuild components of the human heart. *Science*. 2019;365(6452):482-487.
http://science.sciencemag.org/.

27. Remaggi G, Catanzano O, Quaglia F, Elviri L. Alginate self-crosslinking ink for 3D extrusion-based cryoprinting and application for epirubicin-HCl delivery on MCF-7 cells. *Molecules*. 2022;27(3):882.
doi: 10.3390/molecules27030882

28. Sardelli L, Tunesi M, Briatico-Vangosa F, Petrini P. 3D-reactive printing of engineered alginate inks. *Soft Matter*. 2021;17(35):8105-8117.
doi: 10.1039/d1sm00604e

29. Kim E, Seok JM, Bae SB, Park SA, Park WH. Silk fibroin enhances cytocompatibilty and dimensional stability of alginate hydrogels for light-based three-dimensional bioprinting. *Biomacromolecules*. 2021;22(5):1921-1931.
doi: 10.1021/acs.biomac.1c00034

30. Falcone G, Mazzei P, Piccolo A, et al. Advanced printable hydrogels from pre-crosslinked alginate as a new tool in semi solid extrusion 3D printing process. *Carbohydr Polym*. 2022;276:118746.
doi: 10.1016/j.carbpol.2021.118746

31. Guagliano G, Volpini C, Camilletti J, et al. Internally crosslinked alginate-based bioinks for the fabrication of *in vitro* hepatic tissue models. *Biofabrication*. 2023;15(3):035018.
doi: 10.1088/1758-5090/acd872

32. Guagliano G, Volpini C, Sardelli L, et al. Hep3Gel: a shape-shifting extracellular matrix-based, three-dimensional liver model adaptable to different culture systems. *ACS Biomater Sci Eng*. 2023;9(1):211-229.
doi: 10.1021/ACSBIOMATERIALS.2C01226

33. Guagliano G, Volpini C, Sardelli L, Briatico Vangosa F, Visai L, Petrini P. Bioinspired bioinks for the fabrication of chemomechanically relevant standalone disease models of hepatic steatosis. *Adv Healthc Mater*. 2024;13(14):e2303349.
doi: 10.1002/ADHM.202303349

34. Bouhadir KH, Lee KY, Alsberg E, Damm KL, Anderson KW, Mooney DJ. Degradation of partially oxidized alginate and its potential application for tissue engineering. *Biotechnol Prog*. 2001;17(5):945-950.
doi: 10.1021/bp010070p

35. Liberski A, Latif N, Raynaud C, Bollensdorff C, Yacoub M. Alginate for cardiac regeneration: from seaweed to clinical trials. *Glob Cardiol Sci Pract*. 2016;2016(1):e201604.
doi: 10.21542/gcsp.2016.4

36. Łabowska MB, Cierluk K, Jankowska AM, Kulbacka J, Detyna J, Michalak I. A review on the adaption of alginate-gelatin hydrogels for 3D cultures and bioprinting. *Materials*. 2021;14(4):1-28.
doi: 10.3390/ma14040858

37. Cattelan G, Guerrero Gerbolés A, Foresti R, et al. Alginate formulations: current developments in the race for hydrogel-

based cardiac regeneration. *Front Bioeng Biotechnol*. 2020;8:414.
doi: 10.3389/fbioe.2020.00414

38. Roche CD, Lin H, Huang Y, et al. 3D bioprinted alginate-gelatin hydrogel patches containing cardiac spheroids recover heart function in a mouse model of myocardial infarction. *Bioprinting*. 2023;30:e00263.
doi: 10.1016/j.bprint.2023.e00263

39. Sonaye SY, Ertugral EG, Kothapalli CR, Sikder P. Extrusion 3D (Bio)printing of alginate-gelatin-based composite scaffolds for skeletal muscle tissue engineering. *Materials*. 2022;15(22):7945.
doi: 10.3390/ma15227945

40. Heid S, Becker K, Byun J, et al. Bioprinting with bioactive alginate dialdehyde-gelatin (ADA-GEL) composite bioinks: time-dependent *in-situ* crosslinking via addition of calcium-silicate particles tunes *in vitro* stability of 3D bioprinted constructs. *Bioprinting*. 2022;26:e00200.
doi: 10.1016/j.bprint.2022.e00200

41. Sarker B, Papageorgiou DG, Silva R, et al. Fabrication of alginate-gelatin crosslinked hydrogel microcapsules and evaluation of the microstructure and physico-chemical properties. *J Mater Chem B*. 2014;2(11):1470-1482.
doi: 10.1039/c3tb21509a

42. Wang LL, Highley CB, Yeh YC, Galarraga JH, Uman S, Burdick JA. Three-dimensional extrusion bioprinting of single- and double-network hydrogels containing dynamic covalent crosslinks. *J Biomed Mater Res A*. 2018;106(4):865-875.
doi: 10.1002/jbm.a.36323

43. Neira-Velàzquez MG, Rodríguez-Hernández MT, Hernández-Hernández E, Ruiz-Martínez AR. Polymer molecular weight measurement. *Handbook of polymer synthesis, characterization, and processing*. 2013;355-366.

44. Pamies R, Schmidt RR, Martínez MDCL and de la Torre JG. The influence of mono and divalent cations on dilute and non-dilute aqueous solutions of sodium alginates. *Carbohydr Polym*. 2010;80(1):248-253.
https://www.researchgate.net/publication/272785338

45. Forgács AF, Papp V, Paul G, et al. Mechanism of hydration and hydration induced structural changes of calcium alginate aerogel. *ACS Appl Mater Interfaces*. 2021;13:2997-3010.
doi: 10.1021/acsami.0c17012

46. Kaklamani G, Cheneler D, Grover LM, Adams MJ, Bowen J. Mechanical properties of alginate hydrogels manufactured using external gelation. *J Mech Behav Biomed Mater*. 2014;36:135-142.
doi: 10.1016/j.jmbbm.2014.04.013

47. Daly AC, Critchley SE, Rencsok EM, Kelly DJ. A comparison of different bioinks for 3D bioprinting of fibrocartilage and hyaline cartilage. *Biofabrication*. 2016;8(4):045002.
doi: 10.1088/1758-5090/8/4/045002

48. Wang Q, Backman O, Nuopponen M, Xu C, Wang X. Rheological and printability assessments on biomaterial inks of nanocellulose/photo-crosslinkable biopolymer in light-aided 3D printing. *Front Chem Eng*. 2021;3:723429.
doi: 10.3389/fceng.2021.723429

49. Barceló X, Eichholz KF, Garcia O, Kelly DJ. Tuning the degradation rate of alginate-based bioinks for bioprinting functional cartilage tissue. *Biomedicines*. 2022;10(7):1621.
doi: 10.3390/biomedicines10071621

50. Reakasame S, Boccaccini AR. Oxidized alginate-based hydrogels for tissue engineering applications: a review. *Biomacromolecules*. 2018;19(1):3-21.
doi: 10.1021/acs.biomac.7b01331

51. Gomez CG, Rinaudo M, Villar MA. Oxidation of sodium alginate and characterization of the oxidized derivatives. *Carbohydr Polym*. 2007;67(3):296-304.
doi: 10.1016/J.CARBPOL.2006.05.025

52. Salomonsen T, Jensen HM, Larsen FH, Steuernagel S, Engelsen SB. Direct quantification of M/G ratio from 13C CP-MAS NMR spectra of alginate powders by multivariate curve resolution. *Carbohydr Res*. 2009;344(15):2014-2022.
doi: 10.1016/j.carres.2009.06.025

53. Huamani-Palomino RG, Córdova BM, Elvis Renzo Pichilingue L, Venâncio T, Valderrama AC. Functionalization of an alginate-based material by oxidation and reductive amination. *Polymers (Basel)*. 2021;13(2):1-15.
doi: 10.3390/polym13020255

54. Banks SR, Enck K, Wright M, Opara EC, Welker ME. Chemical modification of alginate for controlled oral drug delivery. *J Agric Food Chem*. 2019;67(37):10481-10488.
doi: 10.1021/acs.jafc.9b01911

55. Sarker B, Singh R, Silva R, et al. Evaluation of fibroblasts adhesion and proliferation on alginate-gelatin crosslinked hydrogel. *PLoS One*. 2014;9(9):e107952.
doi: 10.1371/JOURNAL.PONE.0107952

56. Zhao C, Latif A, Williams KJ, Tirella A. The characterization of molecular weight distribution and aggregation by asymmetrical flow field-flow fractionation of unmodified and oxidized alginate. *React Funct Polym*. 2022;175:105292.
doi: 10.1016/j.reactfunctpolym.2022.105292

57. Wang H, Chen X, Wen Y, et al. A study on the correlation between the oxidation degree of oxidized sodium alginate on its degradability and gelation. *Polymers (Basel)*. 2022;14(9):1679.
doi: 10.3390/polym14091679

58. Kristiansen KA, Tomren HB, Christensen BE. Periodate oxidized alginates: depolymerization kinetics. *Carbohydr Polym*. 2011;86(4):1595-1601.
doi: 10.1016/J.CARBPOL.2011.06.069

59. Larsen BE, Bjørnstad J, Pettersen EO, Tønnesen HH, Melvik JE. Rheological characterization of an injectable alginate gel system. *BMC Biotechnol*. 2015;15(1):29.
doi: 10.1186/s12896-015-0147-7

60. Mccain ML, Lee H, Aratyn-Schaus Y, Kléber AG, Parker KK. Cooperative coupling of cell-matrix and cell–cell adhesions in cardiac muscle. *Biophys Comput Biol*. 2012;109(25):9881-9886.
doi: 10.1073/pnas.1203007109/-/DCSupplemental

61. Deddens JC, Sadeghi AH, Hjortnaes J, et al. Modeling the human scarred heart *in vitro*: toward new tissue engineered models. *Adv Healthc Mater*. 2017;6(3):1600571.
doi: 10.1002/adhm.201600571

62. Maxwell CJ, Soltisz AM, Rich WW, Choi A, Reilly MA, Swindle-Reilly KE. Tunable alginate hydrogels as injectable drug delivery vehicles for optic neuropathy. *J Biomed Mater Res A*. 2022;110(10):1621-1635.
doi: 10.1002/jbm.a.37412

63. Park H, Lyons J, Ohtsubo T, Song CW. Acidic environment causes apoptosis by increasing caspase activity. *Br J Cancer*. 1999;80:1892-1897
doi: 10.1038/sj.bjc.6690617

64. Mirek A, Belaid H, Barranger F, et al. Development of a new 3D bioprinted antibiotic delivery system based on a cross-linked gelatin-alginate hydrogel. *J Mater Chem B*. 2022;10(43):8862-8874.
doi: 10.1039/d2tb01268e

65. Li Z, Liao Y, Li D, et al. Design and properties of alginate/gelatin/cellulose nanocrystals interpenetrating polymer network composite hydrogels based on *in situ* cross-linking. *Eur Polym J*. 2023;201:112556
doi: 10.21203/rs.3.rs-2215053/v1

66. Saarai A, Kasparkova V, Sedlacek T, Saha P. On the development and characterisation of crosslinked sodium alginate/gelatine hydrogels. *J Mech Behav Biomed Mater*. 2013;18:152-166.
doi: 10.1016/j.jmbbm.2012.11.010

67. Hackenhaar CR, Rosa CF, Flores EEE, Santagapita PR, Klein MP, Hertz PF. Development of a biocomposite based on alginate/gelatin crosslinked with genipin for β-galactosidase immobilization: performance and characteristics. *Carbohydr Polym*. 2022;291:119483.
doi: 10.1016/j.carbpol.2022.119483

68. Karakaya E, Schöbel L, Zhong Y, et al. How to determine a suitable alginate for biofabrication approaches using an extensive alginate library? *Biomacromolecules*. 2023;24(7):2982-2997.
doi: 10.1021/acs.biomac.2c01282

69. Zehnder T, Sarker B, Boccaccini AR, Detsch R. Evaluation of an alginate-gelatine crosslinked hydrogel for bioplotting. *Biofabrication*. 2015;7(2):025001.
doi: 10.1088/1758-5090/7/2/025001

70. Bociaga D, Bartniak M, Grabarczyk J, Przybyszewska K. Sodium alginate/gelatine hydrogels for direct bioprinting-the effect of composition selection and applied solvents on the bioink properties. *Materials*. 2019;12(7):2669.
doi: 10.3390/ma12172669

71. Li Z, Huang S, Liu Y, et al. Tuning alginate-gelatin bioink properties by varying solvent and their impact on stem cell behavior. *Sci Rep*. 2018;8(1):8020.
doi: 10.1038/s41598-018-26407-3

72. Mondal A, Gebeyehu A, Miranda M, et al. Author correction: characterization and printability of sodium alginate -gelatin hydrogel for bioprinting NSCLC co-culture. *Sci Rep*. 2020;10(1):1732.
doi: 10.1038/s41598-020-58952-1

73. Distler T, Mcdonald K, Heid S, Karakaya E, Detsch R, Boccaccini AR. Ionically and enzymatically dual cross-linked oxidized alginate gelatin hydrogels with tunable stiffness and degradation behavior for tissue engineering. *ACS Biomater Sci Eng*. 2020;6(7): 3899-3914.
doi: 10.1021/acsbiomaterials.0c00677

74. Bider F, Miola M, Clejanu CE, et al. 3D bioprinting of multifunctional alginate dialdehyde (ADA)–gelatin (GEL) (ADA-GEL) hydrogels incorporating ferulic acid. *Int J Biol Macromol*. 2024;257:128449.
doi: 10.1016/j.ijbiomac.2023.128449

75. Genç H, Hazur J, Karakaya E, et al. Differential responses to bioink-induced oxidative stress in endothelial cells and fibroblasts. *Int J Mol Sci*. 2021;22(5):2358.
doi: 10.3390/IJMS22052358

76. Wu Y, Yuan L, Sheng N, et al. A soft tissue adhesive based on aldehyde-sodium alginate and amino-carboxymethyl chitosan preparation through the Schiff reaction. *Front Mater Sci*. 2017;11(3):215-222.
doi: 10.1007/S11706-017-0392-X

77. Emami Z, Ehsani M, Zandi M, Foudazi R. Controlling alginate oxidation conditions for making alginate-gelatin hydrogels. *Carbohydr Polym*. 2018;198: 509-517.
doi: 10.1016/j.carbpol.2018.06.080

78. Dalheim M, Vanacker J, Najmi MA, Aachmann FL, Strand BL, Christensen BE. Efficient functionalization of alginate biomaterials. *Biomaterials*. 2016;80:146-156.
doi: 10.1016/J.BIOMATERIALS.2015.11.043

79. Boontheekul T, Kong HJ, Mooney DJ. Controlling alginate gel degradation utilizing partial oxidation and bimodal molecular weight distribution. *Biomaterials*. 2005;26:2455-2465.
doi: 10.1016/j.biomaterials.2004.06.044

80. Cuomo F, Cofelice M, Lopez F. Rheological characterization of hydrogels from alginate-based nanodispersion. *Polymers (Basel)*. 2019;11(2):259.
doi: 10.3390/polym11020259

81. Cooke ME, Rosenzweig DH. The rheology of direct and suspended extrusion bioprinting. *APL Bioeng*. 2021;5(1):011502.
doi: 10.1063/5.0031475

82. Schwab A, Levato R, D'este M, Piluso S, Eglin D, Malda J. Printability and shape fidelity of bioinks in 3D bioprinting. *Chem Rev*. 2020;120(19):11028-11055. doi: 10.1021/acs.chemrev.0c00084

83. Zhao Y, Li Y, Mao S, Sun W, Yao R. The influence of printing parameters on cell survival rate and printability in microextrusion-based 3D cell printing technology. *Biofabrication*. 2015;7(4):045002. doi: 10.1088/1758-5090/7/4/045002

84. Malekpour A, Chen X. Printability and cell viability in extrusion-based bioprinting from experimental, computational, and machine learning views. *J Funct Biomater*. 2022;13(2):40. doi: 10.3390/jfb13020040

85. Kim E, Seok JM, Bae S Bin, Park SA, Park WH. Silk fibroin enhances cytocompatibilty and dimensional stability of alginate hydrogels for light-based three-dimensional bioprinting. *Biomacromolecules*. 2021;22(5):1921-1931. doi: 10.1021/acs.biomac.1c00034

86. Li A, Guo C, Li X, Li P, Yang X, Guo Y. Gelation mechanism and physical properties of glucono-δ-lactone induced alginate sodium/casein composite gels. *Food Hydrocoll*. 2021;118:106775. doi: 10.1016/J.FOODHYD.2021.106775

87. Jia J, Richards DJ, Pollard S, et al. Engineering alginate as bioink for bioprinting. *Acta Biomater*. 2014;10(10):4323-4331. doi: 10.1016/j.actbio.2014.06.034